Reappraising elastic thickness variation at oceanic trenches

Madeleine Bry[1] and Nicky White[1]

Received 28 November 2005; revised 14 February 2007; accepted 22 March 2007; published 18 August 2007.

[1] We reassess the variation of elastic thickness as a function of lithospheric plate age using a global database of bathymetric and free-air gravity profiles which are perpendicular to oceanic trenches. As in many previous studies, our starting point is the well-known floating elastic plate model. In order to remove the influence of short-wavelength features not associated with lithospheric bending, adjacent profiles from 10-Myr bins have been stacked together to construct average profiles with standard deviations. Each average profile was then inverted in a two-stage procedure. First, singular value decomposition was used to determine two unknown flexural parameters, together with a regional slope and offset, for any given elastic thickness. This procedure was repeated for a range of elastic thicknesses. Second, residual misfit was plotted as a function of elastic thickness, and the global minimum was identified. This two-stage procedure makes no prior assumptions about magnitude of the load, size of the bending moment, or whether the elastic plate is broken/continuous. We obtained excellent fits between theory and observation for both bathymetric and gravity profiles from lithosphere with an age range of 0–150 Ma. The shape of the residual misfit function indicates the degree of confidence we have in our elastic thickness estimates. The lower limit of elastic thickness is usually well determined but upper limits are often poorly constrained. Inverse modeling was carried out using a range of profile lengths (250–300, 500, and 700 km). In general, our estimates show no consistent increase of elastic thickness as a function of plate age. This surprising result is consistent with recent reassessments of elastic thickness beneath seamounts and implies either that elastic thickness is independent of plate age or that elastic thickness cannot be measured with sufficient accuracy to reveal such a relationship. Modeling of short free-air gravity profiles (250–300 km) does tentatively suggest that elastic thickness increases linearly from 5 to 10 km between 0 and 20 Ma and from 10 to 15 km between 20 and 150 Ma. This variation roughly matches the depth to the 200°C isotherm which corresponds to an homologous temperature of 0.4 for wet peridotite. Unfortunately, for longer profile lengths, there is no temporal dependence, and elastic thicknesses vary considerably for all plate ages. Bathymetric profile modeling yields similar results although uncertainties are larger.

Citation: Bry, M., and N. White (2007), Reappraising elastic thickness variation at oceanic trenches, *J. Geophys. Res.*, *112*, B08414, doi:10.1029/2005JB004190.

1. Introduction

[2] In contrast with the vigorous debate about elastic thickness estimates of continental lithosphere, the elastic thickness of oceanic lithosphere T_e is thought to behave in a simple and predictable fashion [*Watts*, 2001, and references therein]. It is widely accepted that elastic thickness increases as a function of plate age because oceanic lithosphere cools, thickens, and strengthens away from the midoceanic ridge [e.g., *Watts*, 1978, 2001; *Caldwell and Turcotte*, 1979; *McNutt and Menard*, 1982; *Burov and Diament*, 1995]. The principal observational support for this attractive hypothesis comes from bathymetric and free-air gravity measurements at trenches and seamounts, which suggest that elastic thickness increases systematically as a function of plate age at time of loading. When plotted against plate age, the envelope of T_e values is bounded by the 300°–600°C isotherms which delimits the mechanically strong part of the lithospheric plate [*Watts et al.*, 1980; *Bodine et al.*, 1981; *Cloetingh and Burov*, 1996]. Although a scatter in the T_e-age relationship has always been evident, inconsistencies have usually been attributed to thermal anomalies [e.g., *Watts*, 2001].

[3] These observational results are broadly corroborated by our understanding of the material properties of minerals and rocks. The rheological behavior of a material is principally controlled by τ, the ratio of its temperature to its melting temperature, both measured in kelvin [*Ashby and Verrall*, 1977; *Weertman*, 1978]. τ effectively controls the

[1]Bullard Laboratories, Department of Earth Sciences, University of Cambridge, Cambridge, UK.

0148-0227/07/2005JB004190$09.00

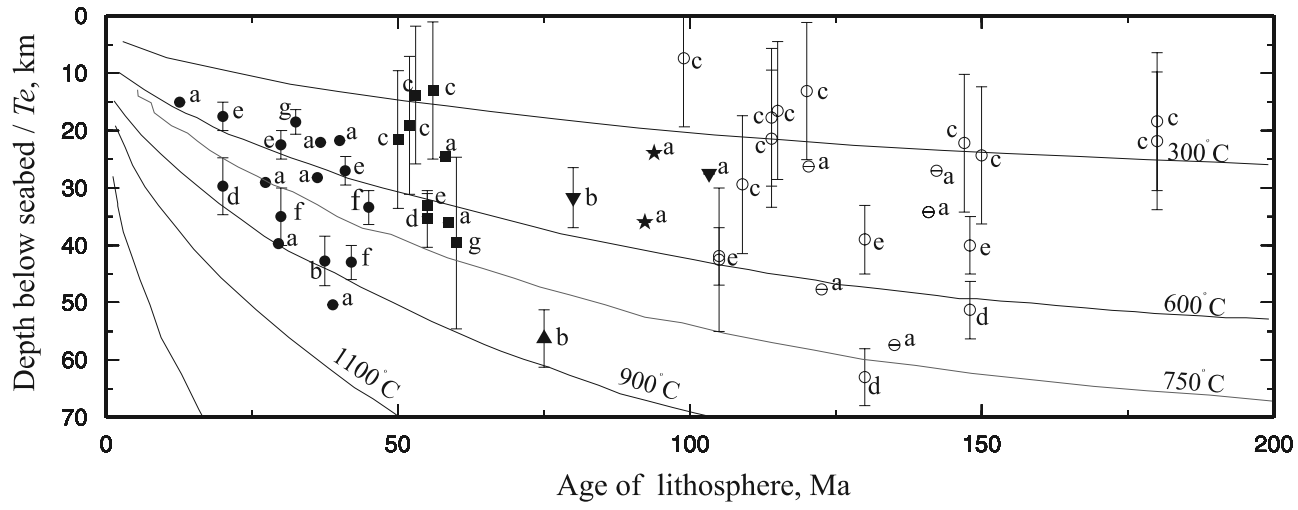

Figure 1. Elastic thickness T_e as a function of age of oceanic lithosphere compiled from previous studies of oceanic trench profiles. (a) Analyses of *Levitt and Sandwell* [1995], (b) *McAdoo et al.* [1985], (c) *McQueen and Lambeck* [1989], (d) *McAdoo and Martin* [1984], (e) *McNutt* [1984], (f) *Judge and McNutt* [1991], (g) *Caldwell and Turcotte* [1979]. Filled circles, analyses from Middle America and Peru-Chile trenches; filled squares, Aleutian Trench; filled triangle, South Sandwich Trench; filled inverted triangles, Caribbean Trench; filled stars, Java Trench; and open circles, Kuril-Bonin-Marianas trenches. Labeled solid lines, isothermal boundaries redrawn from the work of *Watts* [2001].

transition timescale from elastic to plastic behavior, and materials can only maintain elastic stresses over geologic time if τ is less than $\sim$0.4. If the rheology of oceanic lithosphere is controlled by dry peridotite (i.e., olivine), τ = 0.4 roughly corresponds to the 450°C isotherm [*Watts*, 1978]. In both the oceans and continents, T_e measurements tend to be smaller than the observed seismogenic thickness which is consistent with viscoelastic behavior on a timescale of 0–2 Ma [*Bodine et al.*, 1981; *Watts*, 2001; *McKenzie et al.*, 2005].

[4] Bending of oceanic lithosphere has been modeled using a large range of rheologies which include elastic [*Caldwell et al.*, 1976], elastic-plastic [*Goetze and Evans*, 1979], viscous [*De Bremaecker*, 1977], or multilayered viscoelastic [*Courtney and Beaumont*, 1983; *Watts and Zhong*, 2000] models. Unfortunately, trench profiles cannot easily be used to discriminate between these different models. *Forsyth* [1980] and *Bodine et al.* [1981] convincingly demonstrated that profiles can be modeled equally well by simple elastic and by multilayered rheological models. The main reason for using more sophisticated elastic-plastic rheologies is to tackle the problem of unrealistically large shear stresses which are predicted by the elastic model when curvatures exceed $\sim 10^{-6}\,m^{-1}$. By incorporating the effects of inelastic yielding using a yield stress envelope, any T_e measurement can be converted into T_m, the true mechanical thickness (i.e., T_e at zero curvature) [*McNutt and Menard*, 1982; *McNutt*, 1984; *Watts*, 2001]. T_m is always greater than T_e. However, this transposition is predicated upon the validity of yield stress envelopes which unfortunately depend upon extrapolation of laboratory data by over 10 orders of magnitude.

[5] Our reappraisal of elastic thickness as a function of plate age is only concerned with plate deflections at oceanic trenches, which reliably sample a wide range of oceanic crustal ages from 0 to 160 Ma [*Müller et al.*, 1997]. We do not revisit the more challenging problem of estimating elastic thicknesses for seamounts [e.g., *Watts*, 1978; *Calmant*, 1987; *Watts et al.*, 2006; *Crosby*, 2006]. The main complications with seamounts are poor determination of plate age at time of loading and poor quantification of surface and subsurface components of the load. In many cases, bathymetry is also poorly known. Bending at trenches is viewed as a more tractable problem where plate age is easily determined and where the load can be more reasonably characterized as a simple line load. Trenches have been the subject of numerous previous studies; the results of which are compiled in Figure 1. However, published studies differ both in the type and quality of data as well as in modeling strategies, both of which makes direct comparison of different T_e estimates difficult. For example, *Caldwell et al.* [1976] and *Caldwell and Turcotte* [1979] modeled the bathymetry of trenches by measuring the distance from the first-zero crossing (measured from the crossing of an arbitrary local depth) to the outer rise peak. They concluded that the effective elastic thickness corresponds satisfactorily to the depth of the 700°C isotherm. *McNutt* [1984] measured the height of the flexural bulge and the wavelength of the first zero crossing from individual bathymetry profiles in order to estimate the moment and curvature of the deflection assuming an elastic plate model. Her approach suggests a scattered relationship between T_e and the age of the oceanic lithosphere which is improved by converting T_e into T_m using the curvature of the plate. The distribution of inferred T_m values suggests that the base of the mechanical lithosphere is defined by the 600°C isotherm for a 125-km-thick thermal plate model [*McNutt*, 1984]. *McAdoo and Martin* [1984] and *McAdoo et al.* [1985] used the Seasat geoid database to model the flexural wavelength of the deflection with a thin plate elastic model. They found that

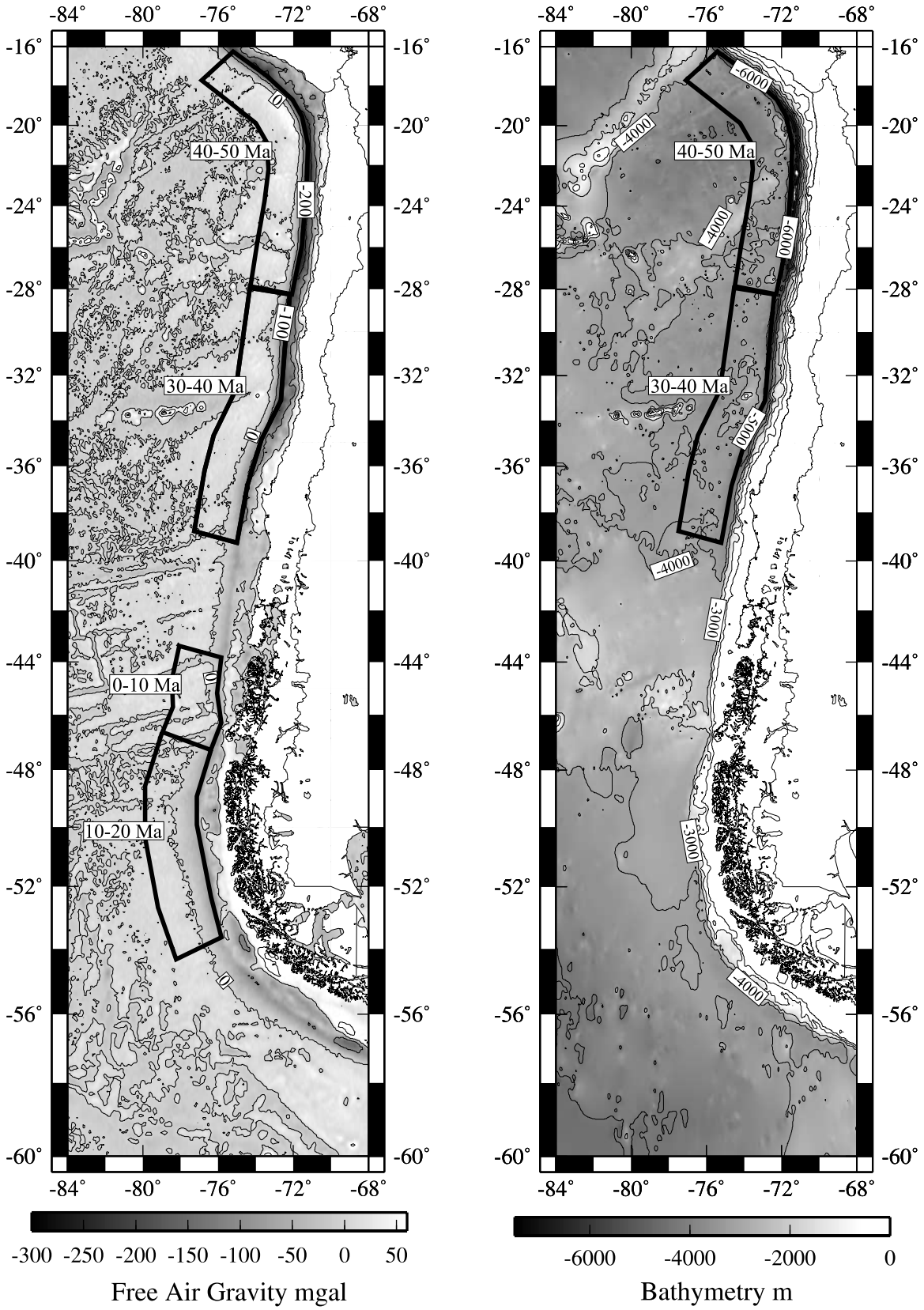

Figure 2. Maps of Chile Trench. Left-hand panel, free-air gravity map from the work of *Sandwell and Smith* [1992] where age-labeled boxes indicate regions over which gravity profiles have been averaged as discussed in text. Right-hand panel, bathymetric map showing age-labeled boxes over which bathymetric profiles have been averaged as discussed in text. Subsequent maps are organized in the same fashion.

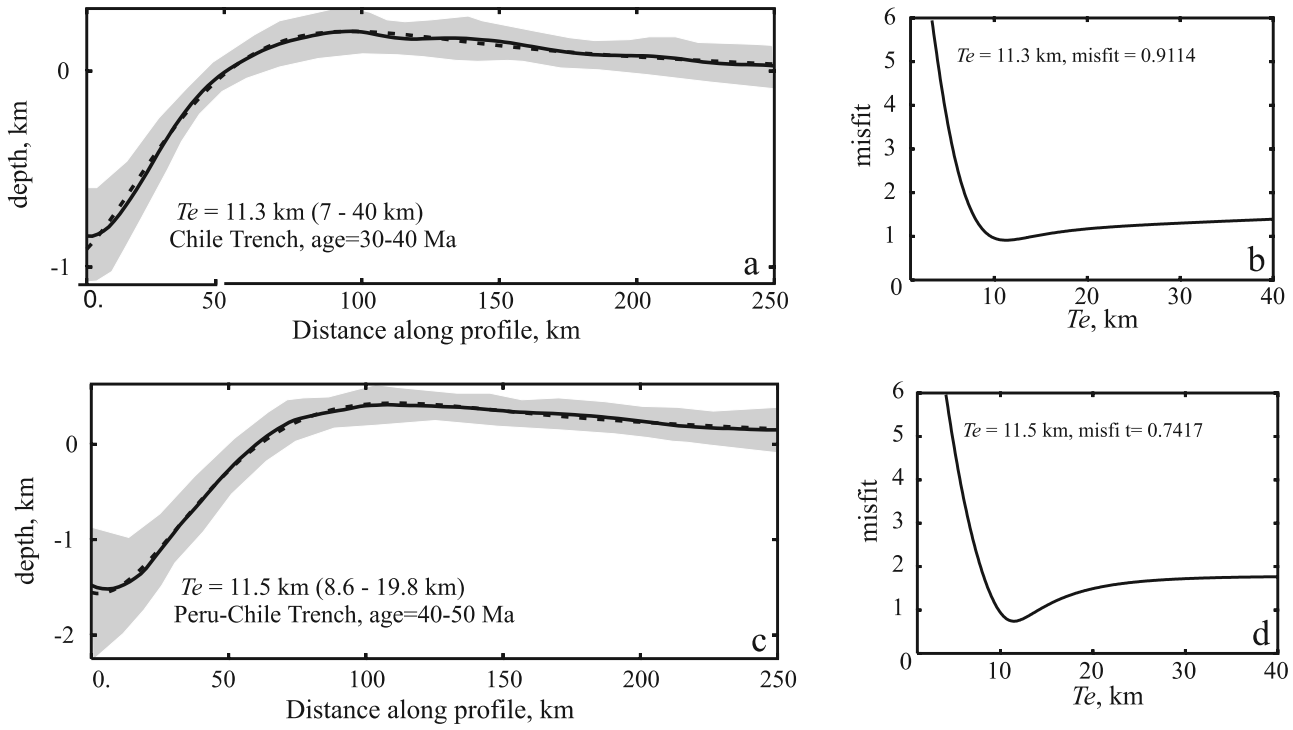

Figure 3. Results of inverse modeling of bathymetric profiles from Chile Trench for two lithospheric plate age ranges shown in Figure 2 (30–40 and 40–50 Ma). (a, c) Fitted bathymetric profiles: solid line, average bathymetric profile with indicated age range; grey zone, two standard deviations; dashed line, best fitting theoretical curve obtained by combination of singular value decomposition and multiple forward modeling as described in text; T_e values, best fit and estimated range of elastic thickness. (b, d) Misfits between observed and theoretical curves plotted as a function of T_e; values of T_e and residual misfit at global minimum are given. Note the shape of misfit function which constrains the lower limit of T_e but does not, in general, constrain upper limit. Subsequent inverse modeling plots are organized in the same fashion.

the equivalent T_e values correlate with the square root of lithospheric age. *McQueen and Lambeck* [1989] used an iterative least squares method which simultaneously minimizes flexural parameters such as flexural wavelength, α, first-zero crossing, and regional slope. This method was applied to bathymetric profiles from the Marianas, Japan, Kuril, and Aleutian trenches using average profile lengths of 600 km or greater. These authors find considerable scatter in the relationship between T_e and lithospheric age. They suggested that there was only a mild tendency for plate strength to increase with age, following the 200°–300°C isotherm. They also asserted that T_e cannot be accurately determined in many cases because of the long and short-wavelength noise in bathymetric measurements which is unrelated to flexure. *Judge and McNutt* [1991] used a database of gravity, geoid, and bathymetric measurements to estimate T_e and plate curvature for the Peru and Chile trenches. They modeled profile lengths of ~500 km using a simple elastic model and showed the fits obtained. Their results show that major changes in elastic thickness can occur along a trench and that the 800°C isotherm defines the base of the mechanical lithosphere.

[6] The most recent global synthesis was carried out by *Levitt and Sandwell* [1995] who inverted a combined data set of free-air gravity and age-corrected bathymetric measurements using a simple elastic model. Their T_e estimates are considerably scattered and do not obviously track a particular isotherm. This scatter is thought to be caused by a combination of nonflexural features in bathymetric profiles and inelastic bending. They converted T_e estimates into T_m values which suggests that the thickness of the mechanical lithosphere thickens with time. However, the large amount of scatter precludes isolation of any particular thermal model (for example, the plate cooling models of *Parsons and Sclater* [1977]; *Stein and Stein* [1992]). *Levitt and Sandwell* [1995] showed all the free-air gravity and bathymetric profiles which they have jointly inverted. The quality of fit and the degree of residual misfit can be assessed in each case, although misfit functions are not plotted. We have three reasons for revisiting this popular problem. First, although we are using similar data sets to *Levitt and Sandwell* [1995], we have inverted free-air gravity and bathymetric profiles separately rather than together. We also stack profiles instead of modeling them separately in order to mitigate short-wavelength, nonflexural effects. Second, although we also use the simple elastic model, our inversion strategy is different from many others (it is similar to that of *McQueen and Lambeck*, 1989). In particular, we construct misfit as a function of elastic thickness in order to assess uncertainty in our elastic thickness estimates. Third, there remains considerable controversy and confusion about the

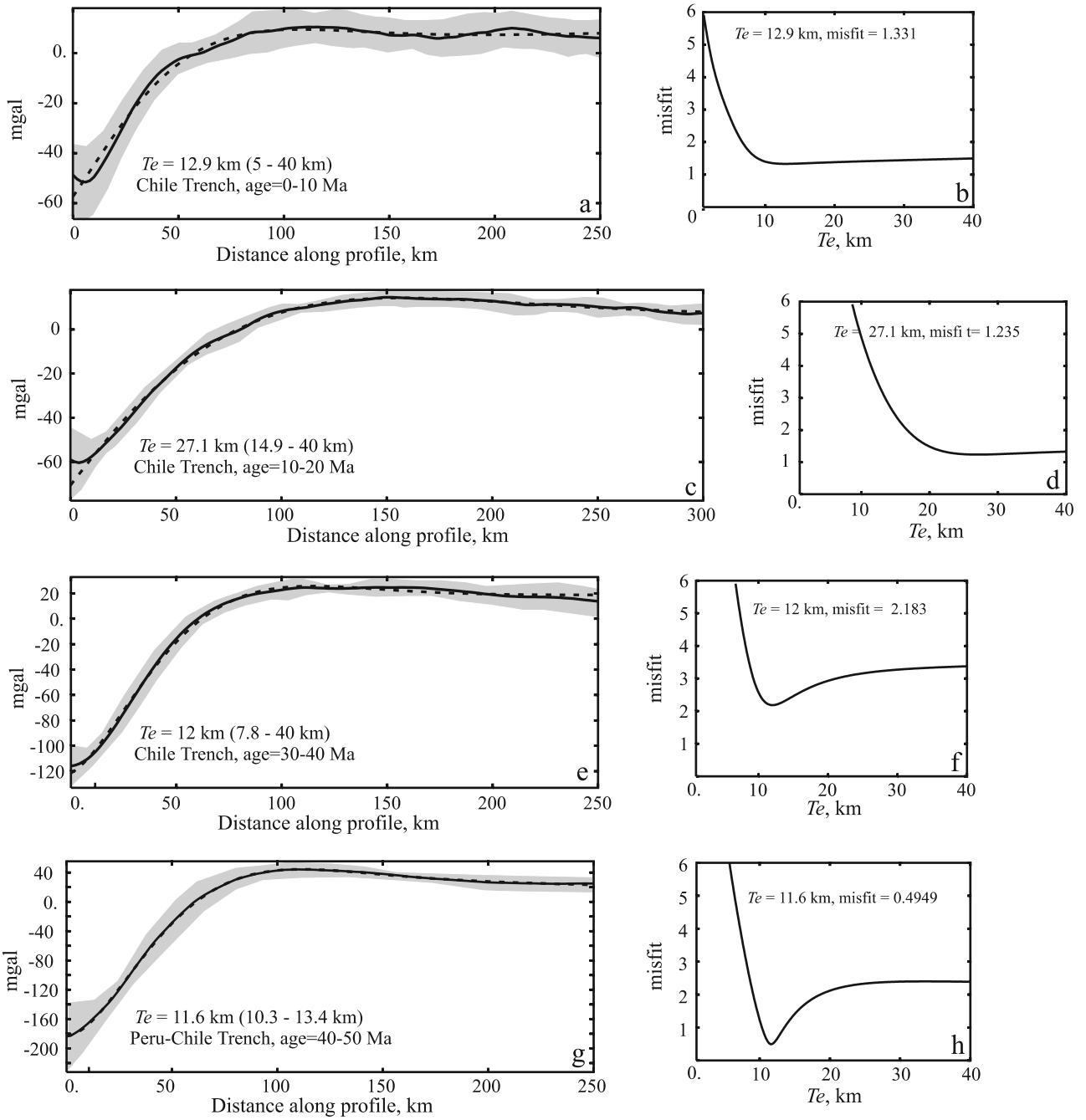

Figure 4. Results of inverse modeling of free-air gravity profiles from Chile Trench for four lithospheric plate age ranges shown in Figure 2 (0–10, 10–20, 30–40, and 40–50 Ma). (a, c, e, and g) Fitted free-air gravity profiles; (b, d, f, and h) misfit functions. See caption of Figure 3 for details.

whole concept of T_e in the continents. Appeals are often made to the fact that oceanic lithosphere obeys simple rules, whereas the continents do not. It is timely to revisit the oceanic problem.

2. Modeling Strategy

[7] The simplest model for estimating elastic thickness assumes that oceanic lithosphere can be treated as a uniform elastic beam of length x [e.g., *Turcotte and Schubert*, 1982; *Watts*, 2001]. This beam rests upon an inviscid substrate and can be subjected to point or distributed loads. Here we assume a point load $V_\circ$ which is applied at $x = 0$. If the thin sheet approximation is used and if there are no horizontal forces, deflection of the beam as a function of distance, $w(x)$, away from the load is given by

$$D\frac{d^4w}{dx^4} + \Delta\rho g w = 0 \tag{1}$$

where D is the flexural rigidity of the beam, $\Delta\rho$ is the density contrast between the substrate and the material

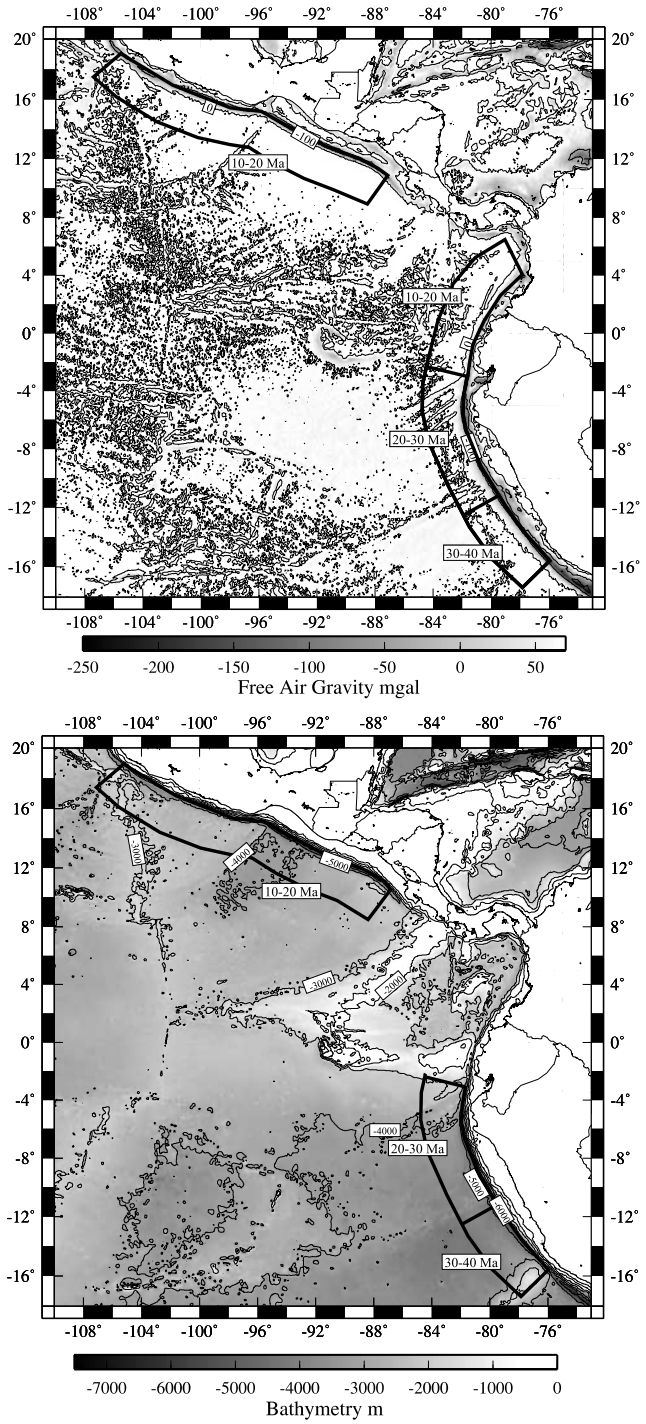

Figure 5. Maps of Columbia-Peru and Middle America trenches. Upper panel, free-air gravity map with age-labeled boxes; lower panel, bathymetric map with age-labeled boxes.

surrounding the load, and g is gravitational acceleration. Given that $w \rightarrow 0$ as $x \rightarrow \infty$, the general solution of equation (1) for $x > 0$ reduces to

$$w(x) = a_1 \exp\left(-\frac{x}{\alpha}\right)\cos\left(\frac{x}{\alpha}\right) + a_2 \exp\left(-\frac{x}{\alpha}\right)\sin\left(\frac{x}{\alpha}\right) \quad (2)$$

where the flexural parameter α is given by

$$\alpha = \left(\frac{4D}{\Delta\rho g}\right)^{\frac{1}{4}} \quad (3)$$

and the relationship between D and T_e is given by

$$D = \frac{ET_e^3}{12(1-\sigma^2)} \quad (4)$$

where $E = 8 \times 10^{10}$ Pa is Young's modulus and $\sigma = 0.25$ is Poisson's ratio. The principal assumptions of this model are that the system is in static equilibrium and that the deformed plate only experiences elastic (i.e., recoverable) strain. The rheology of oceanic lithosphere is undoubtedly more complex. For example, in-plane stresses and strain softening can develop as a result of inelastic failure of the upper crust [e.g., *Burov and Diament*, 1995]. Loading could also be distributed beneath the deflection itself. Unfortunately, bathymetric and gravity measurements alone cannot discriminate between these different possibilities. Our philosophy is to reassess whether or not the simplest possible model can fit a global database of bending observations which is why we follow the strategies of *McQueen and Lambeck* [1989] and *Levitt and Sandwell* [1995] with modification.

[8] From a geophysical perspective, there are two important forms of solution. For a continuous beam, the point load is applied at the center of a beam which is symmetrical about $x = 0$. Thus $dw/dx = 0$ at $x = 0$ which requires that

$$a_1 = a_2 = \frac{V_\circ \alpha^3}{8D} \quad (5)$$

For a broken beam with no applied external torque, $d^2w/dx^2 = 0$ at $x = 0$ which requires that $a_2 = 0$ and

$$a_1 = \frac{V_\circ \alpha^3}{4D} \quad (6)$$

Bending at trenches is often modeled as a broken beam with a bending moment of $M_\circ$ applied at $x = 0$ [e.g., *Parsons and Molnar*, 1976; *Turcotte and Schubert*, 1982]. In this case, the two constants are

$$a_1 = \frac{\alpha^2}{2D}(M_\circ + V_\circ \alpha) \quad (7)$$

and

$$a_2 = \frac{-M_\circ \alpha^2}{2D} \quad (8)$$

Unfortunately, $V_\circ$ and $M_\circ$ cannot be independently measured, and we believe that it is very important not to fix these unknown parameters in advance (contra *Jordan and Watts* [2005] who calculated the size and shape of the load from topography alone and then invert for T_e and the position of the "plate break"). Instead, $V_\circ$ and $M_\circ$ are permitted to vary and we find that there are significant trade-offs between $V_\circ$, $M_\circ$

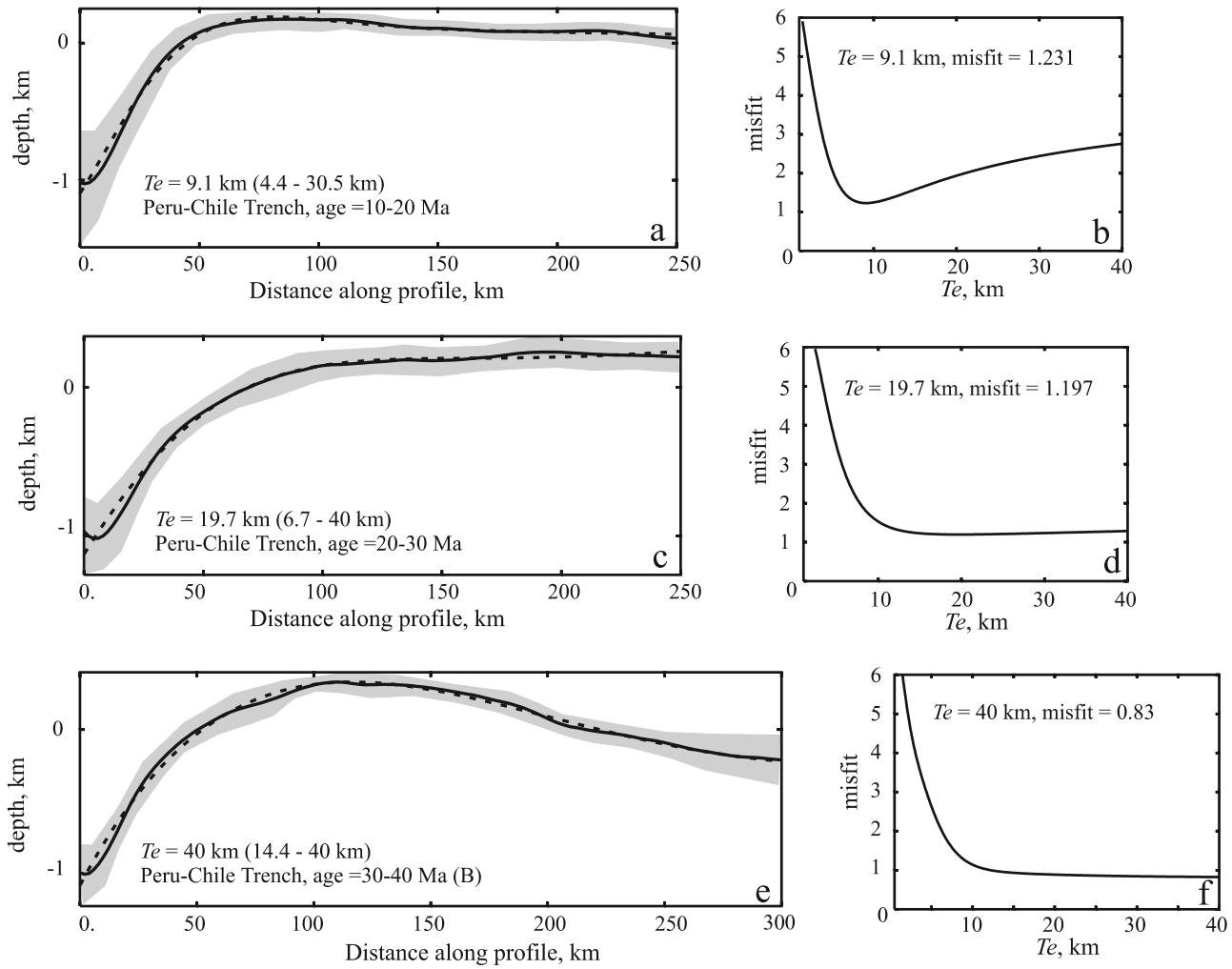

Figure 6. Results of inverse modeling of bathymetric profiles from Peru-Chile Trench for three age ranges shown in Figure 5 (10–20, 20–30, and 30–40 Ma). See Figure 3 for further details.

and, T_e which both moderate the shape of the misfit function and affect the location of its global minimum. In this way, the vexed matter of surficial and subsurficial load characterization is sidestepped. Following the work of *Levitt and Sandwell* [1995] and *McKenzie and Fairhead* [1997], we include two additional terms which correct for regional topographic gradient and for undeflected depth. Thus

$$w(x) = a_1 \exp\left(-\frac{x}{\alpha}\right)\cos\left(\frac{x}{\alpha}\right) + a_2 \exp\left(-\frac{x}{\alpha}\right)\sin\left(\frac{x}{\alpha}\right) + a_3 x + a_4 \tag{9}$$

The equivalent form for the free-air gravity anomaly is

$$\delta g(x) = c_1 \exp\left(-\frac{x}{\alpha}\right)\cos\left(\frac{x}{\alpha}\right) + c_2 \exp\left(-\frac{x}{\alpha}\right)\sin\left(\frac{x}{\alpha}\right) + c_3 x + c_4 \tag{10}$$

where, as before, c_i are constants determined for each profile. We note in passing that our calculated gravity anomalies do not exactly fit observations because we do not include all possible density contrasts.

[9] Bending at oceanic trenches can be modeled using either the free-air gravity anomaly or the bathymetric profile or both [e.g., *Levitt and Sandwell*, 1995]. Bathymetric observations are generally deemed suitable since most trenches are not substantially infilled by sediment and so the bathymetric expression of trench bending is accurately preserved. However, in trenches where sedimentation rates are high (for example, the Chile and Caribbean trenches), bathymetry does not adequately reflect trench bending, and so we think that it is better to fit bathymetric and free-air gravity data sets separately.

[10] Free-air gravity measurements were extracted for each trench from the global grid of satellite radar altimetry data [*Sandwell and Smith*, 1992]. This data set is thought to be accurate for the purposes of flexural modeling since flexural wavelengths are typically greater than the 60-km track spacing of the recording satellite [*Levitt and Sandwell*, 1995]. Bathymetric data have been organized in order to preserve the maximum level of accuracy. Original ship track echo soundings were extracted from a global bathymetric grid using odd integer depth values (D.T. Sandwell, 2000, written communication). This procedure allows us to avoid

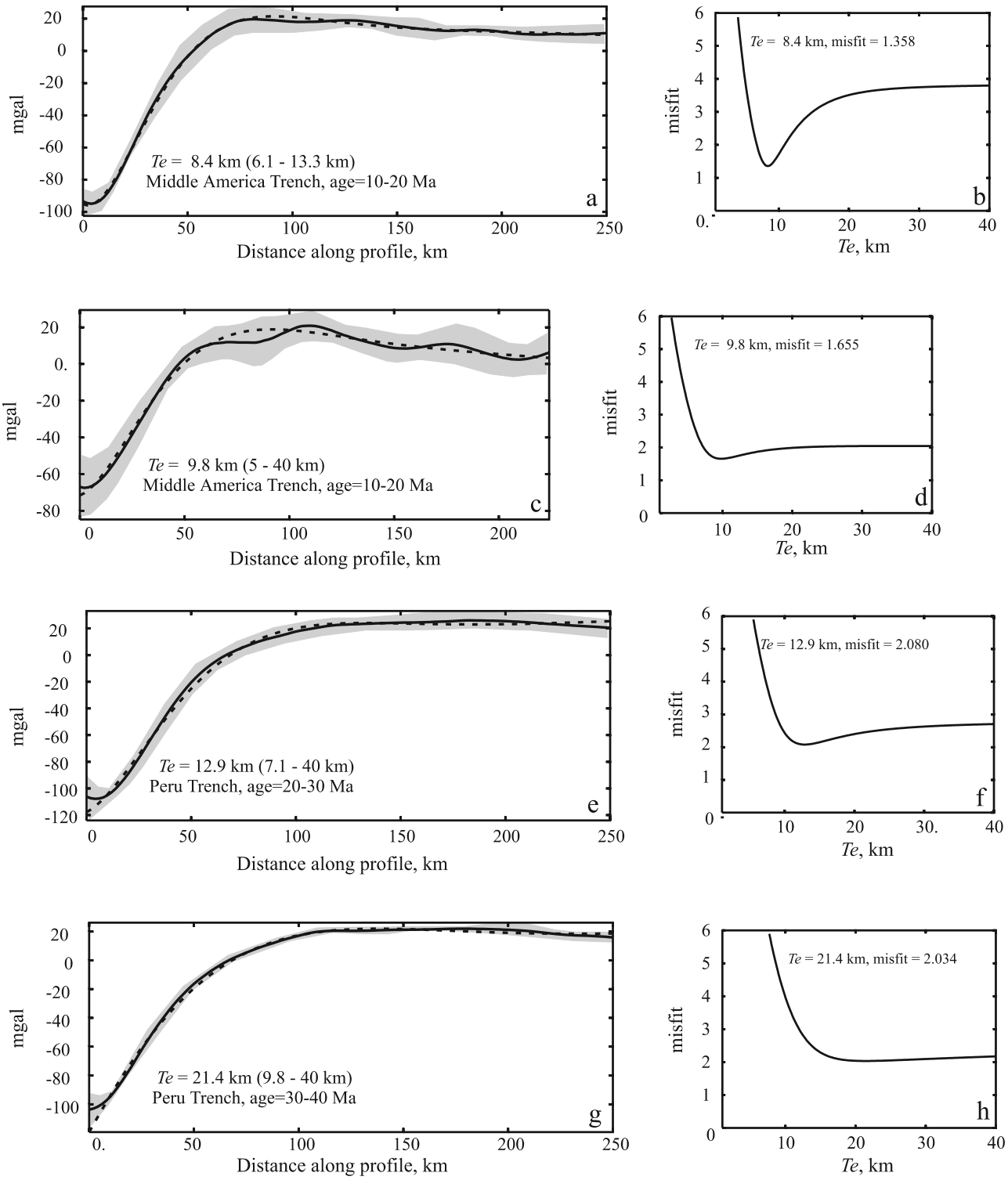

Figure 7. Results of inverse modeling of free-air gravity profiles from Middle America and Peru trenches. (a, b) Fitted free-air gravity profiles for northwest and southeast sectors of box with age range 10–20 Ma shown in Figure 5. (b, d) Equivalent misfit functions. (e, g) Fitted free-air gravity profiles from Peru Trench for two age ranges shown in Figure 5 (20–30 and 30–40 Ma). (f, h) Equivalent misfit functions. See caption of Figure 3 for further details.

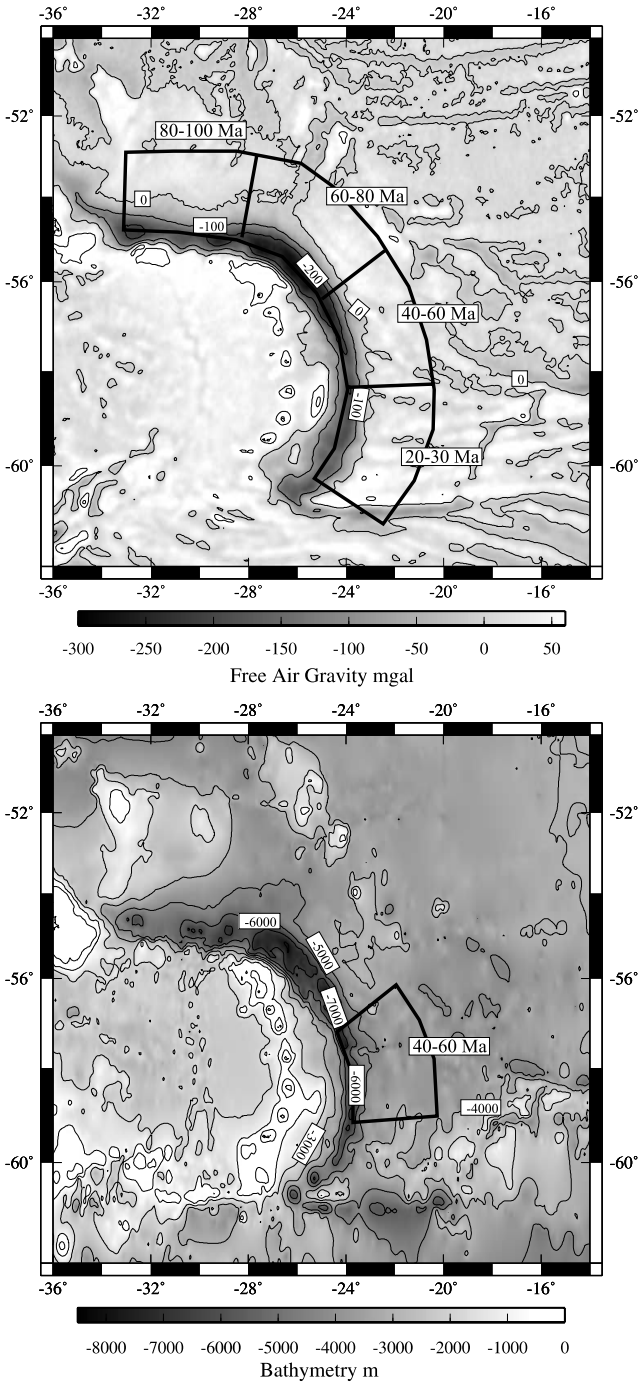

Figure 8. Maps of South Sandwich Trench. Upper panel, free-air gravity map with age-labeled boxes; lower panel, bathymetric map with age-labeled box.

using predicted bathymetry, which has been estimated in part by using the admittance relationship between bathymetry and free-air gravity. Where echo-soundings are densely sampled, they have been regridded to produce a map whence bathymetric profiles can be averaged for T_e modeling. Owing to their proximity to coastlines, most deep-sea trenches are covered by densely sampled underway measurements. However, the density of these measurements is poor at the South Sandwich Trench, at the southern part of the Tonga Trench, at part of the Java Trench, and at a small part of the Marianas Trench. We have not used bathymetric data from these portions of trenches. In contrast with previous analyses, we have paid particular attention to generating average profiles for each portion of trench. There are two reasons for averaging profiles. First, most trenches have significant short-wavelength bathymetric and gravity features which are not related to flexure. In our view, it is better to remove these features before modeling. Second, by averaging large numbers of profiles, the standard deviation can be calculated and used to weight the data during the inversion procedure. Each oceanic trench was divided into age bins of 10 Ma which were taken from the digital age grid of *Müller et al.* [1997]. These bins were picked where decimal isochrons intersect the trace of a given trench, and we show them for all bathymetric and free-air gravity maps. Profiles are averaged within each bin but where isochrons are too closely spaced; no trench profiles are modeled. A set of profiles is defined perpendicular to a line through the maximum of a trench deflection. Spacing between profiles ranges from 10 to 20 km, and their lengths are chosen so that the whole flexural feature is observed. An average profile is then constructed by calculating the mean of all points of each individual profile at the same distance from the zero point. A constant offset is applied to each profile to ensure that its mean is the same as the average mean, and a scale factor is applied to minimize the RMS difference between each profile and the mean. In this way, standard deviations at each point along a profile can be estimated from scaled profiles. Although we only show modeled profiles which are 250–300 km in length, we have also analyzed sets of longer profiles (i.e., 500 and 700 km) and a small number of individual profiles in order to allow comparison with the results of *Judge and McNutt* [1991] and *Levitt and Sandwell* [1995]. All profiles have been modeled using the same density contrast on either side of the plate ($\Delta\rho$ = 2300 kg m^{-3}).

[11] Following *McQueen and Lambeck* [1989], *Judge and McNutt* [1991], and *Levitt and Sandwell* [1995], we have used an inverse modeling approach. Our strategy differs in several important ways which affects the shape of the misfit function and thus the quality of T_e estimates. For a succession of elastic thicknesses at T_e intervals of 100 m, the four parameters a_1-a_4 are found by minimizing a misfit function H, which measures the difference between the observed and theoretical profile such that

$$H^2 = \frac{1}{N}\sum\left[\frac{h_n - w(x_n)}{\sigma_n}\right]^2 \qquad (11)$$

N is the number of points along the profile, h_n is the height of the nth point of the average profile, and σ_n is its standard deviation calculated during profile averaging. In this way, the minimal misfit versus T_e is obtained whose global minimum yields that T_e which produces a best match between theoretical and observed profiles. In order to minimize the misfit, a_1, a_2, a_3, and a_4 must be such that all partial derivatives $\delta H/\delta a_{1-4}$ are equal to 0. These simultaneous equations are solved by singular value decomposition [*Press et al.*, 1986]. This method does not consider trade-

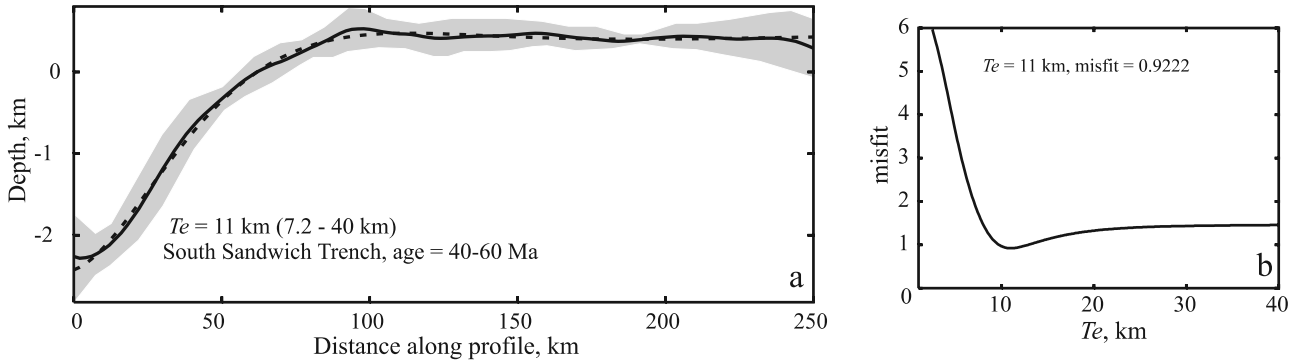

Figure 9. Results of inverse modeling of bathymetric profiles from South Sandwich Trench for single lithospheric plate age range shown in Figure 8 (40–60 Ma is the only box with reliable ship track data). (a) Fitted bathymetric profiles; (d) misfit plotted as a function of T_e.

offs between a_1-a_4 and T_e which fortunately are negligible. The uncertainty in T_e is taken to be 1.25 H_{min}.

[12] As many others have shown, bending stresses that are induced by flexure at the top of the plate are given by

$$\sigma_{xx} = \frac{6M}{T_e^2} \tag{12}$$

where the bending moment $M(x)$ at a distance x along the profile is

$$M(x) = -D\frac{d^2w}{dx^2} \tag{13}$$

[13] The maximum curvature of the plate can be calculated given the maximum allowable bending stresses which are used to estimate T_m [*McNutt*, 1984].

3. Results

[14] We present results from a global analysis of bathymetric and gravity data sets. Our analysis has three main aims. First, coverage of the oceanic realm is as complete as possible and includes back-arc systems. Second, inverse modeling of all profiles has been carried out in a consistent fashion. Third, the uncertainty in each estimates of T_e has been calculated in a simple and transparent way.

3.1. Peru-Chile-Middle America Trenches

[15] The Chile, Peru, and Middle America trenches extend from southernmost Chile to Mexico and include oceanic crust ranging in age from 0 to 50 Ma. The Chile-Peru Trench is a manifestation of subduction of the Nazca Plate beneath the South American Plate, whereas the Middle America Trench indicates subduction of the Cocos Plate beneath the North American Plate. These trenches are densely covered with ship track data, except at the southern extremity of the Chile Trench (south of 54°S). In any case, the trench south of 40°S has virtually no bathymetric expression, probably owing to infill by sediment from rivers along the Chilean margin, which are not present further north because of the aridity of the climate (Figure 2b). Consequently, we have no T_e estimate from bathymetric profiles for the 0- to 10- and 10- to 20-Ma boxes of the Chile Trench. There is also very little flexural expression in the bathymetry between 2°S and 10°N, possibly due to complex interactions with the Cocos and Carnegie ridges and due to sediment input toward the Panama Basin (Figure 5).

[16] Bathymetric profile modeling results for 30- to 40- and 40- to 50-Ma boxes at the Chile Trench are shown in Figure 3. In both cases, the average bathymetric profiles are accurately fitted using an elastic thickness of 11 km. Despite the existence of global minima in both cases, the misfit functions demonstrate that higher elastic thicknesses are plausible, hence the large error estimates. Satellite altimetric coverage allows a more complete analysis of the free-air gravity data. Apart from one sector at 42°S where fracture zones cause complications, all of the Chile Trench can be analyzed (Figure 4). Averaged free-air gravity profiles from four boxes can be accurately fitted and can show that T_e does not vary significantly over an age range of 0–50 Ma. In fact, the 10- to 20-Ma box yields a minimal T_e of 27 km which is nearly double of the values from younger and older boxes.

[17] The results of analyzing a set of boxes from the Peru and Middle America trenches are shown in Figures 6 and 7. Bathymetric profiles indicate that the best fit T_e varies between 9 and 20 km with the 20- to 30-Ma box, showing that T_e could be as low as 7 km with no upper limit. Free-air gravity profiles yielded better constrained results. Three boxes, spanning 10–30 Ma, yield T_e of approximately 10 km. The 30- to 40-Ma box gives a higher value of 21 km.

[18] In summary, free-air gravity profile modeling along South and Middle America yields better constrained values of T_e than bathymetric modeling. In many cases, T_e values range between ~8 and 27 km, but most bins yield T_e values around 11–13 km, which do not appear to change with the age of the section. The largest value from these trenches comes from gravity modeling of the Chile Trench for age range 10–20 Ma. This anomalously high value probably reflects shallowing of the negative gravity anomaly due to sediment infill (Figure 4). Where both global minima are reasonably well constrained, free-air gravity and bathymetric profiles yield similar results (for

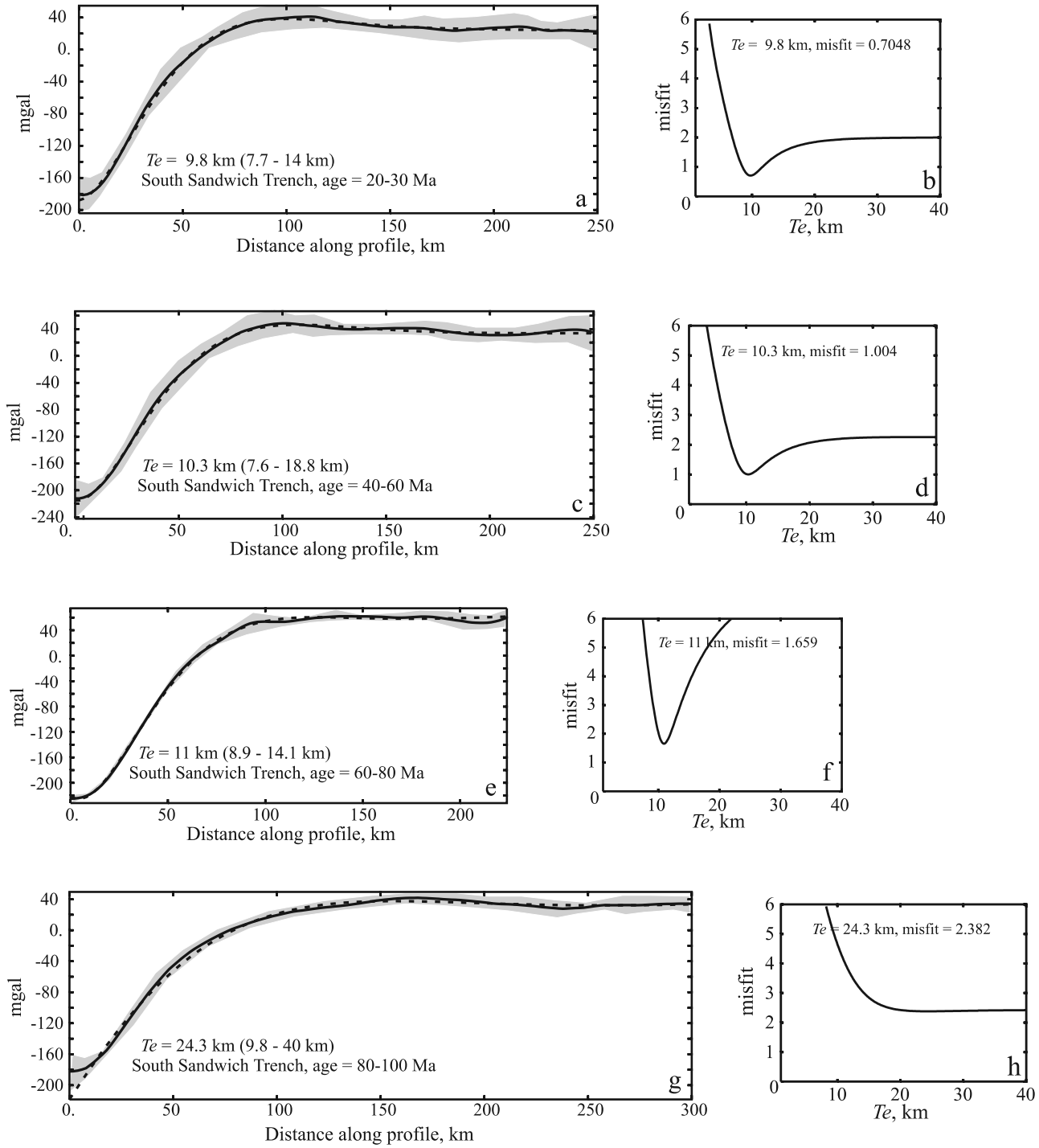

Figure 10. Results of inverse modeling of free-air gravity profiles from South Sandwich Trench for four lithospheric plate age ranges shown in Figure 8 (20–30, 40–60, 60–80, and 80–100 Ma). (a, c, e, and g) Fitted free-air gravity profiles; (b, d, f, and h) misfit functions. See caption of Figure 3 for further details.

example, 10- to 20-Ma box of Middle America Trench and 30- to 40-, 40- to 50-Ma boxes of Chile Trench). Elsewhere, one of the two results is poorly constrained (for example, 20- to 30- and 30- to 40-Ma boxes of Chile-Peru Trench even though the wavelengths of the free-air gravity and bathymetric anomalies are similar, which suggests that T_e values should be similar).

3.2. South Sandwich Trench

[19] The narrow South Sandwich Trench is located at the eastern end of the Scotia Plate and is a consequence of

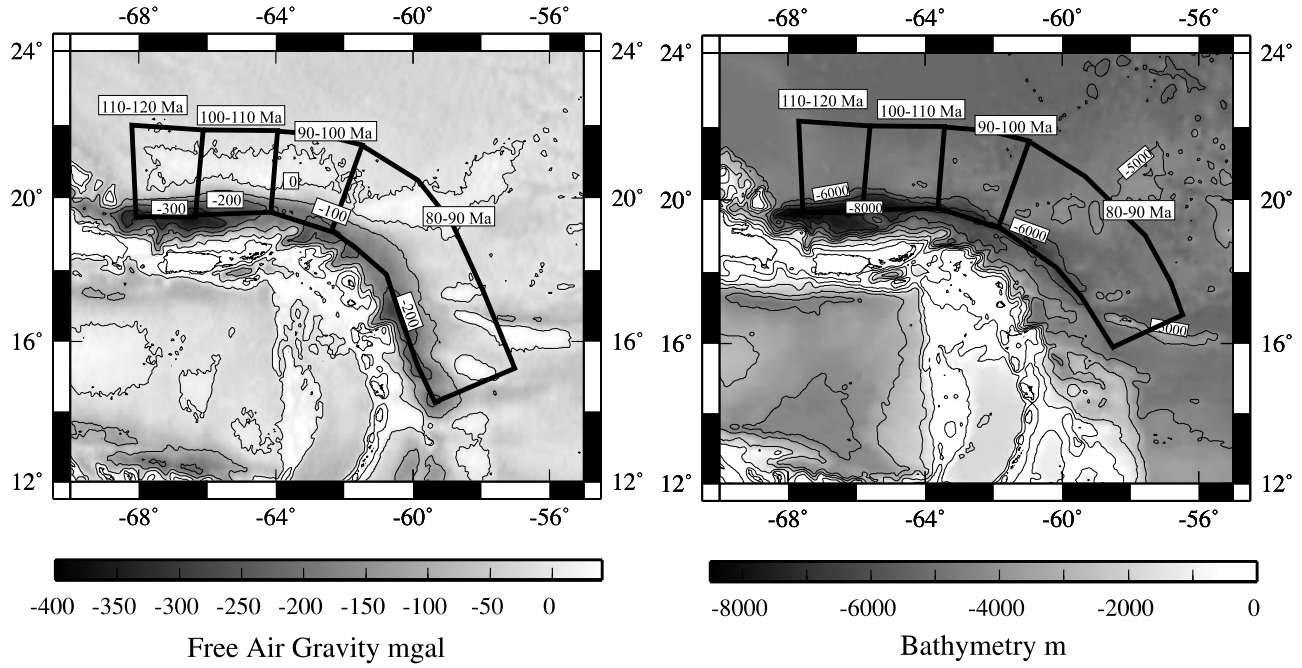

Figure 11. Maps of Caribbean Trench. Left-hand panel, free-air gravity map with age-labeled boxes; right-hand panel, bathymetric map with age-labeled boxes.

subduction of the South American Plate beneath the Scotia Plate. This trench features oceanic crust ranging from 20 to 100 Ma, and we have divided it into four boxes (Figure 8). It is a remote region with sparse ship track data, and only one box has sufficient bathymetric tracks amenable to stacking (Figure 9a).

[20] The three youngest boxes (20–30, 40–60, and 60–80 Ma) yield reasonably well-constrained T_e values from free-air gravity profiles; the best fit values barely increase with age from 9.8 to 10.3 and 11 km (Figure 10). This modest increase is obviously not well resolved. The bathymetric profile for age range 40–60 Ma yields a consistent T_e of 11 km. A significant change occurs for the 80- to 100-Ma box where T_e increases to ~24 km. This high value is partly a consequence of the poor upper limit on T_e evident from the misfit function. Nevertheless, the wavelength of the gravity anomaly increases from ~100 km for the 60- to 80-Ma section to ~150 km for this oldest section, implying that the rapid increase in T_e is real. Not enough is known about the South Sandwich Trench to explain this change by sediment infilling.

3.3. Caribbean Trench

[21] At the Caribbean Trench, bending oceanic lithosphere of the North American Plate ranges in age from 80 to 120 Ma (Figure 11). This region is very densely sampled by ship tracks and so four boxes of bathymetric and gravity data can be analyzed which reveal important discrepancies. For example, the bathymetric and free-air gravity expressions of the trench for the 80- to 90-Ma box have markedly different wavelengths, and therefore elastic thicknesses (compare Figures 12a and 13a). This significant discrepancy is probably a consequence of the presence of thick piles of sediment in the southern part of the trench near Barbados in contrast with the deeper, starved sector of the trench further west [*Westbrook*, 1982]. Sediment thickness maps confirm considerable infill of the eastern sector of the trench [*Kaplan et al.*, 1985]. We note that, as for the South Sandwich Trench, the northern segment of this trench near Puerto Rico is essentially a strike-slip boundary. Nevertheless, this boundary must have a component of shortening in order to generate significant bathymetric and gravimetric anomalies.

[22] As before, free-air gravity profile modeling yields well-constrained values of T_e, ranging from 12 to 15.5 km for the three older boxes (90–100, 100–110, and 110–120 Ma). There is no apparent relationship between T_e and crustal age (Figure 13). In fact, the youngest box yields the highest T_e value of ~20 km in agreement with a significant increase in wavelength of the anomaly. As before, this value probably reflects the distribution of thick sediment around the trench, shallowing the negative anomaly because of the sediment's lower density.

[23] Bathymetric modeling generally yields more inconsistent and poorly constrained T_e values, which are not always in agreement with those obtained from free-air gravity data (Figure 12). Bathymetric and gravity values agree well for the oldest box (110–120 Ma), but T_e values from bathymetry are not well constrained for the 100- to 110- and 90- to 100-Ma boxes and the deflections are not satisfactorily fitted. Finally, bathymetric modeling of the youngest box, which yielded an anomalously high value of T_e from free-air gravity modeling, suggests that T_e is as low as ~7 km. This unexpectedly low value could be a consequence of trench sediments forming a wedge in the deeper part of the trench so that bathymetric deflection is

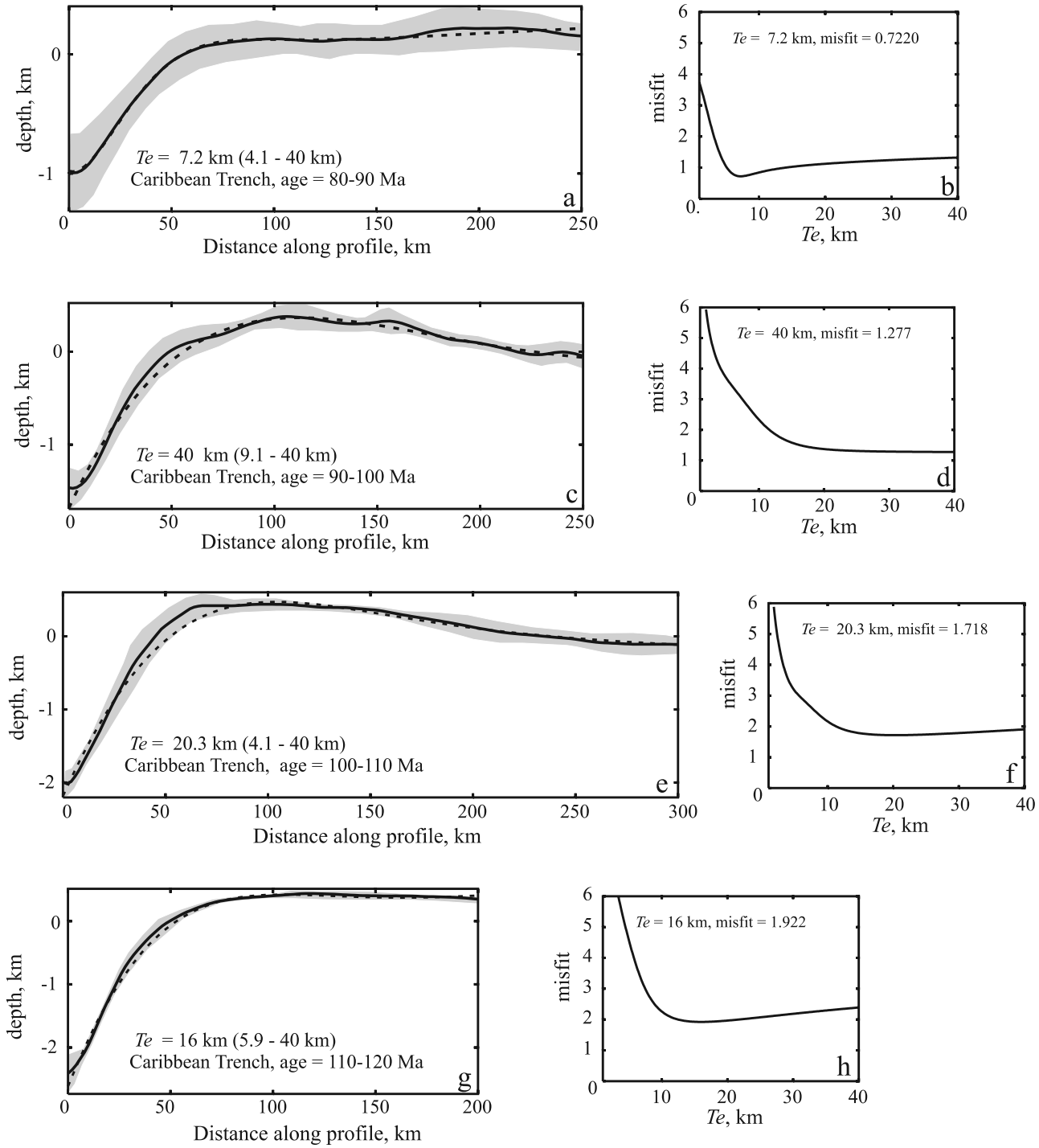

Figure 12. Results of inverse modeling of bathymetric profiles from the Caribbean Trench for four lithospheric plate age ranges shown in Figure 11 (80–90, 90–100, 100–110, and 110–120 Ma). (a, c, e, and g) Fitted bathymetric profiles; (b, d, f, and h) misfit functions. See caption of Figure 3 for further details.

only observed in part. This effect would cause an apparent narrowing of bathymetric expression.

3.4. Aleutian Trench

[24] The long Aleutian Trench has been divided into just two boxes (40–50 and 50–60 Ma; Figure 14). This trench formed as a result of subduction of the Pacific Plate, preceded by the Kula Plate, beneath the North American Plate. It is covered by a dense network of ship track bathymetry [*Levitt and Sandwell*, 1995]. For both bathymetric and free-air gravity data, the older section of trench (50–60 Ma) yields significantly lower T_e values than the younger section (20 and 17 km versus 12 and 13 km; Figures 15 and 16). Once again, these differences reflect

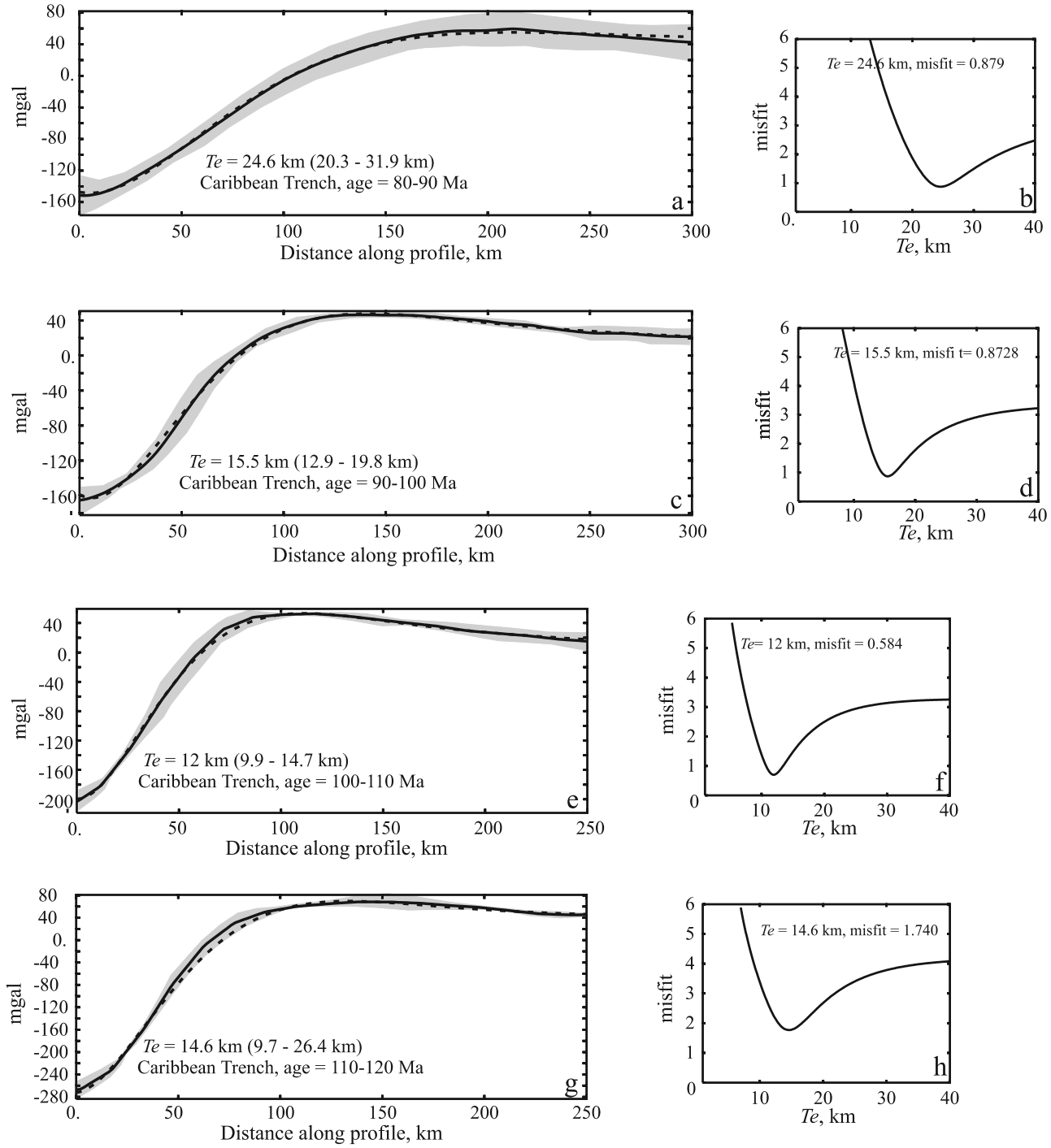

Figure 13. Results of inverse modeling of free-air gravity profiles from the Caribbean Trench for four lithospheric plate age ranges shown in Figure 11 (80–90, 90–100, 100–110, and 110–120 Ma). (a, c, e, and g) Fitted free-air gravity profiles; (b, d, f, and h) misfit functions. See caption of Figure 3 for further details.

changes in the wavelength of bending. Free-air gravity modeling yields better constrained results. For the 40- to 50-Ma box, T_e from bathymetric modeling is virtually unconstrained.

3.5. Kuril-Japan-Marianas Trenches

[25] The combined Kuril, Japan, and Marianas trenches compose the oldest oceanic crust modeled in this study, increasing in age toward the south from 120 to 160 Ma (Figure 17). The Kuril and Japan trenches result from the subduction of the Pacific Plate beneath the Eurasian Plate, while the Marianas Trench records subduction of the Pacific Plate beneath the Philippine Plate. Ship track coverage of the Kuril and Japan trenches is reasonable in contrast with that of the Marianas Trench where bathymetric data are too

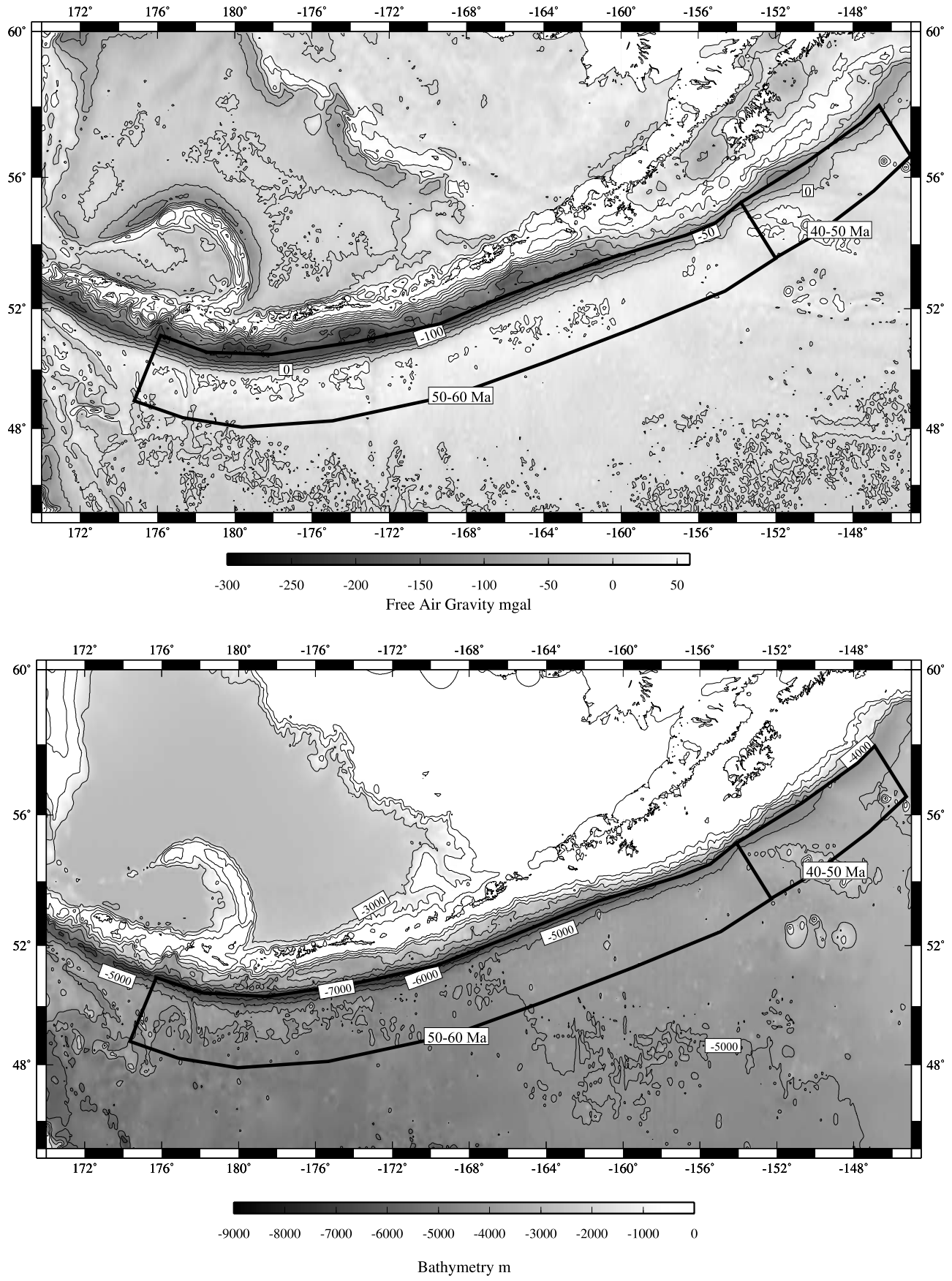

Figure 14. Maps of Aleutian Trench. Upper panel, free-air gravity map with age-labeled boxes; lower panel, bathymetric map with age-labeled boxes.

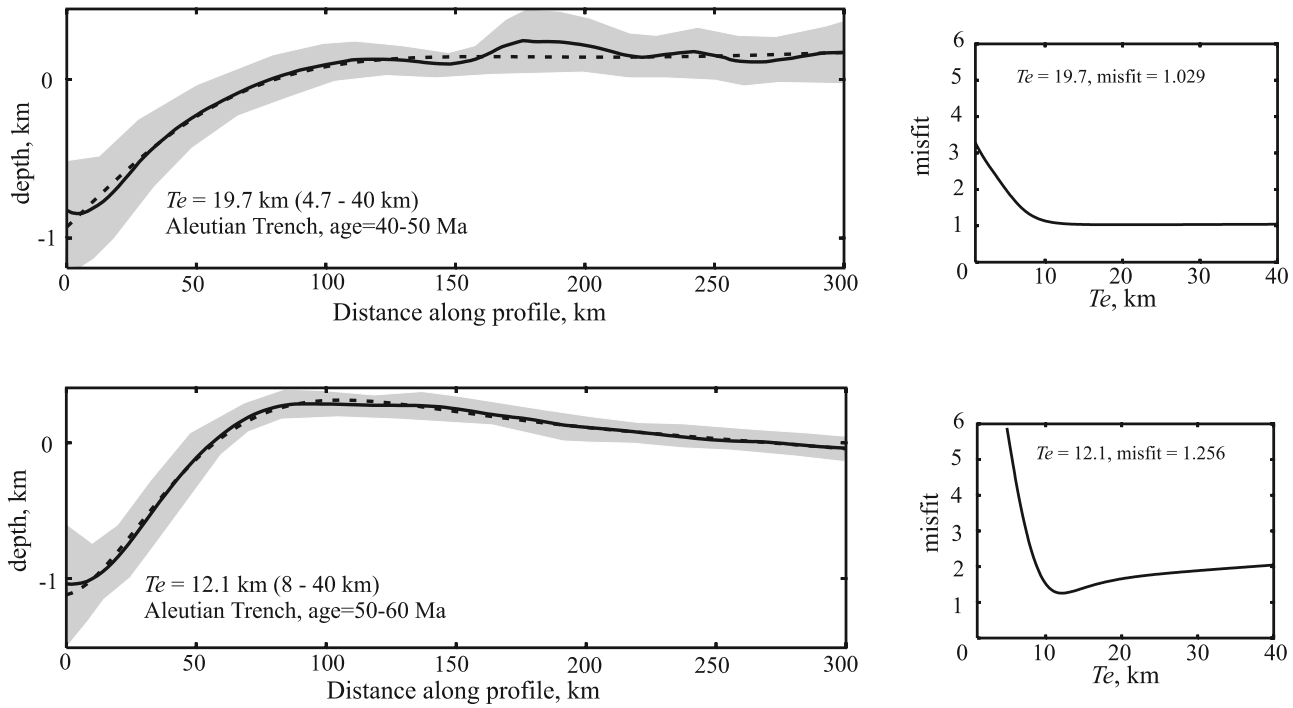

Figure 15. Results of inverse modeling of bathymetric profiles from Aleutian Trench for two lithospheric plate age ranges shown in Figure 4 (40–50 and 50–60 Ma). (a, c) Fitted bathymetric profiles; (b, d) misfit functions. See caption of Figure 3 for further details.

sparse to be modeled between 18° and 24°N and between 142° and 145°E (Figure 17a).

[26] Once again, our results do not indicate a consistent relationship between age of the bending lithosphere and T_e. At Kuril Trench (120–130 Ma), bathymetry and free-air gravity are consistent with a well-constrained T_e of about 14 km (Figures 18a and 19a). The northern part of the Japan Trench (130–140 Ma) yields similar values,

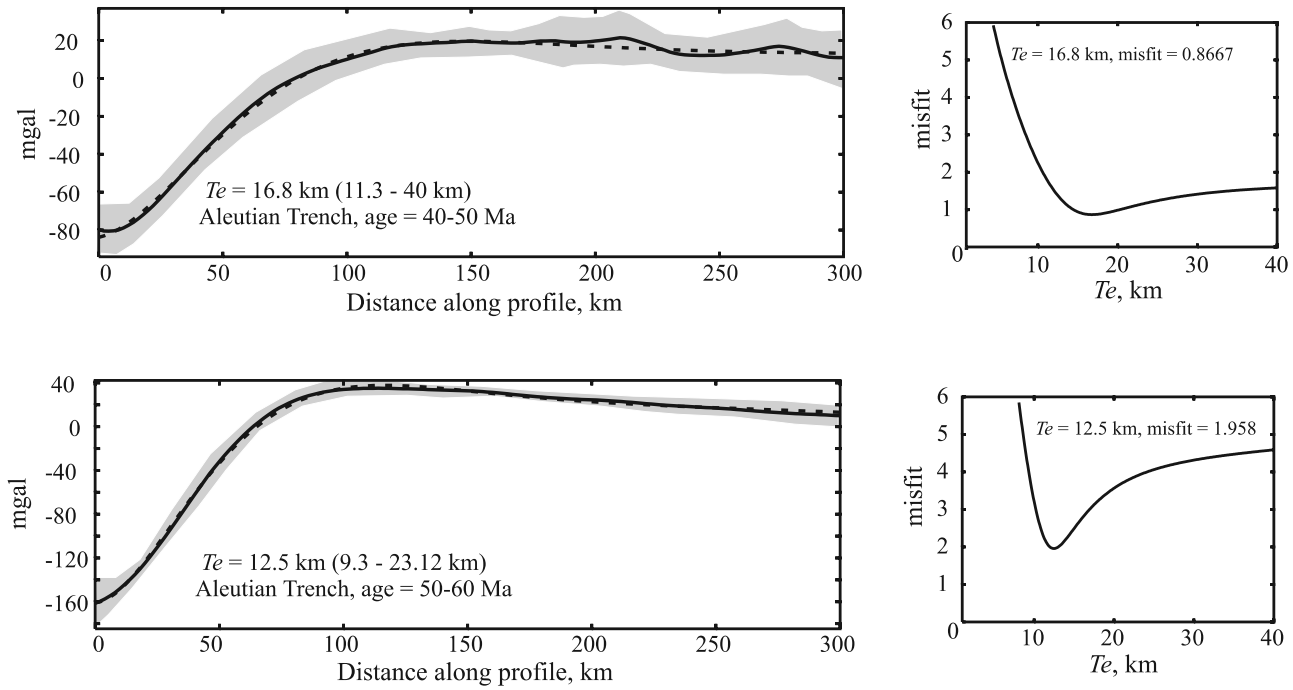

Figure 16. Results of inverse modeling of free-air gravity profiles from Aleutian Trench for two lithospheric plate age ranges shown in Figure 14 (40–50 and 50–60 Ma). (a, c) Fitted free-air gravity profiles; (b, d) misfit functions. See caption of Figure 3 for further details.

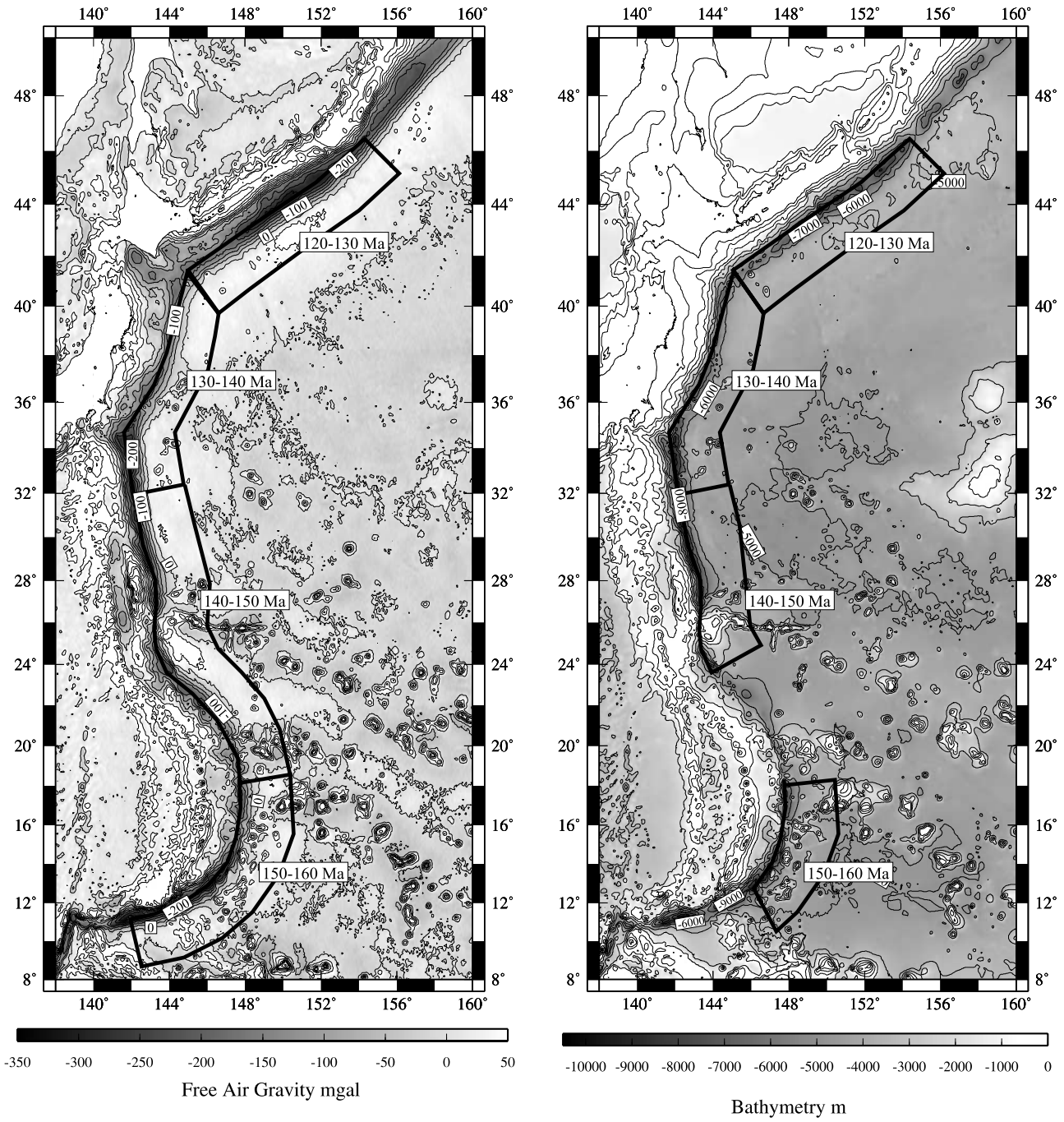

Figure 17. Maps of Kuril, Japan, and Marianas trenches. Left-hand panel, free-air gravity map with age-labeled boxes; right-hand panel, bathymetric map with age-labeled boxes.

although the bathymetric value is poorly constrained (Figures 18b and 19b). The older southern box (140–150 Ma) yields slightly lower values of T_e (11 and 13 km: Figures 18 and 19). The oldest box (150–160 Ma) comprises the Marianas Trench, and once more, free-air gravity and bathymetric profiles yield similar results (T_e of ~16 km).

[27] Given the age of the bending lithosphere, this area has yielded consistently and surprisingly low values of T_e. As before, bathymetric data give less well-constrained values of T_e but they do agree with those determined from free-air gravity modeling.

3.6. Java Trench

[28] The Java Trench is a manifestation of subduction of the Indo-Australian Plate beneath the Eurasian Plate where oceanic lithosphere ranges in age from 40 to 100 Ma (Figure 20). The digital isochron map has considerable data gaps in the area east of 104°E, and so ages for this area has been inferred from the work of *Levitt and Sandwell* [1995]

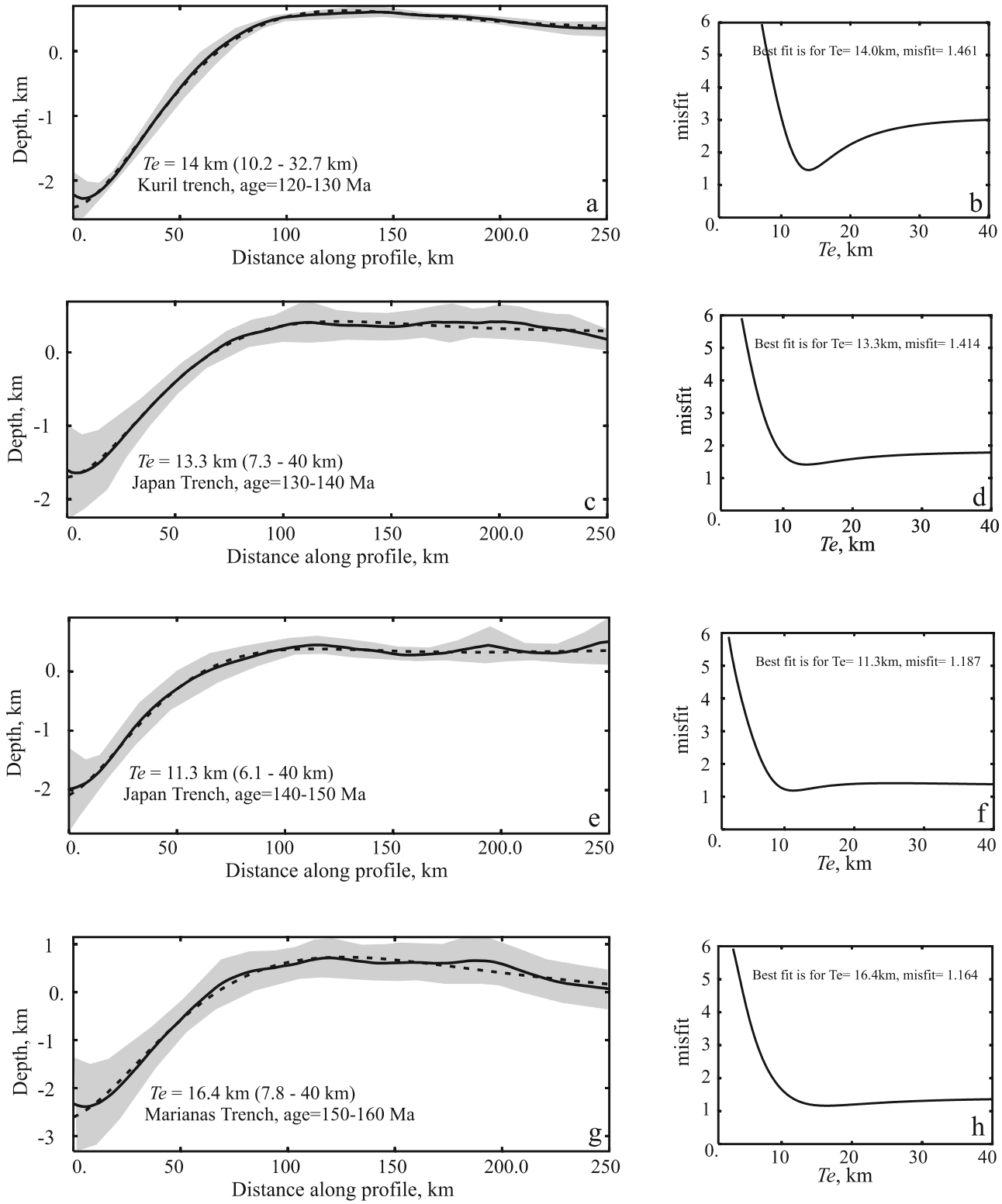

Figure 18. Results of inverse modeling of bathymetric profiles from Kuril, Japan and Marianas trenches for 4 lithospheric plate age ranges shown in Figure 17 (120–130, 130–140, 140–150 and 150–160 Ma). 140–150 and 150–160 Ma boxes have sparse ship track data. (a), (c), (e) and (g) Fitted bathymetric profiles; (b), (d), (f) and (h) Misfit functions. See caption of Figure 3 for further details.

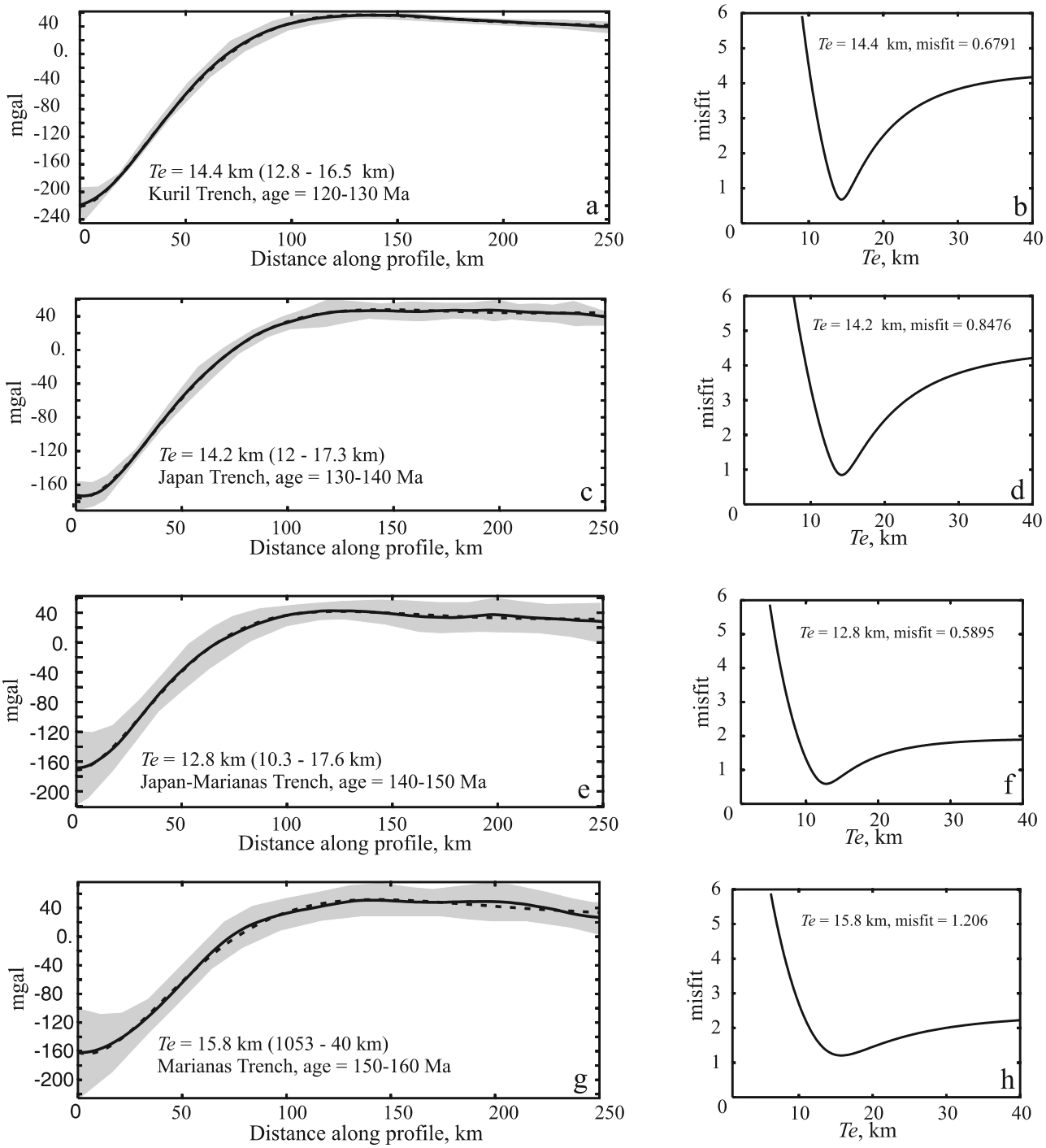

Figure 19. Results of inverse modeling of free-air gravity profiles from Kuril, Japan, and Marianas trenches for four lithospheric plate age ranges shown in Figure 17 (120–130, 130–140, 140–150, and 150–160 Ma). (a, c, e, and g) Fitted free-air gravity profiles; (b, d, f, and h) misfit functions. Wavelength of flexure is similar in each case and so T_e is unlikely to significantly vary. See caption of Figure 3 for further details.

who used an earlier version of the isochron map [*Roest et al.*, 1992]. In general, the Java Trench has a sparse ship track coverage, and only two boxes could be used for bathymetric modeling (Figure 21b). Thus only two of five boxes can be modeled using both free-air gravity and bathymetric profiles, and one of these (40–50 Ma) may not be reliable since it remains very poorly sampled outside the axis of the trench.

[29] The fits obtained using the stacked bathymetric profiles are both poor compared to results from elsewhere. Once again, there is no obvious relationship between age of bending plate and its T_e value (Figures 20c and 20d). The

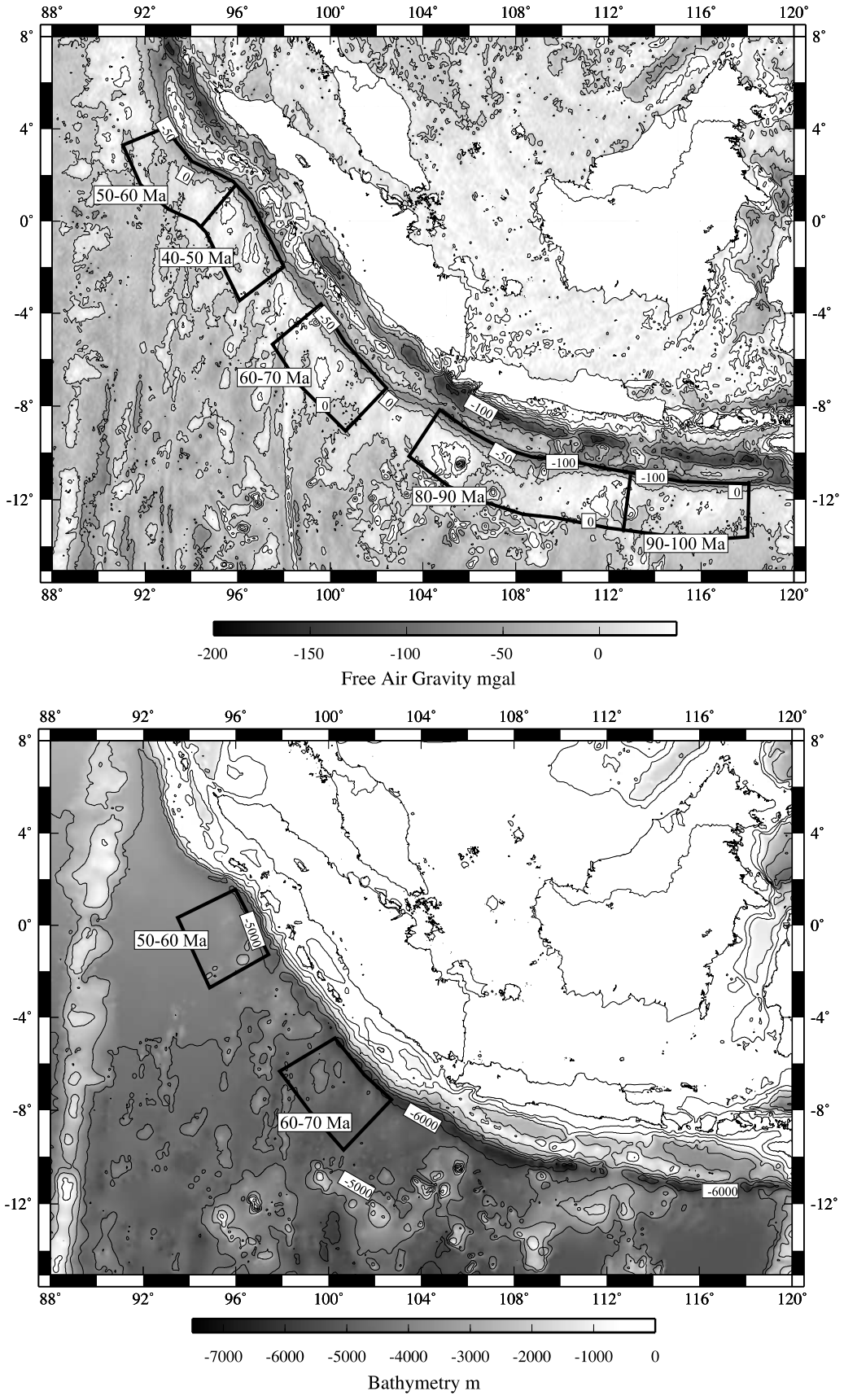

Figure 20. Maps of Java Trench. Upper panel, free-air gravity map with age-labeled boxes; lower panel, bathymetric map with age-labeled boxes. (c, d) Results of inverse modeling of bathymetric profiles from Java Trench.

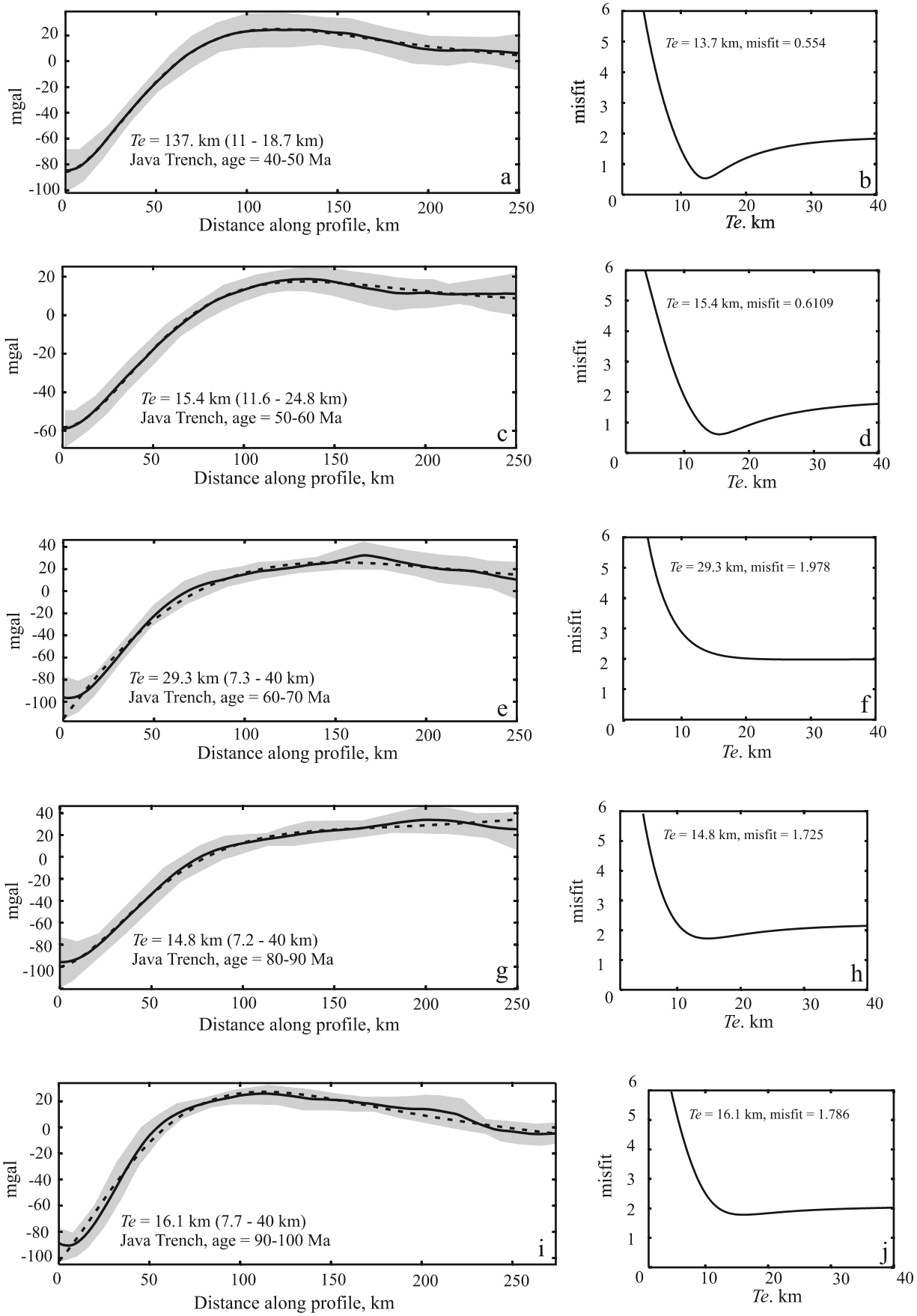
mgal
Te = 137. km (11 - 18.7 km)
Java Trench, age = 40-50 Ma
a
Distance along profile, km
misfit
Te = 13.7 km, misfit = 0.554
b
Te. km
Te = 15.4 km (11.6 - 24.8 km)
Java Trench, age = 50-60 Ma
c
Te = 15.4 km, misfit = 0.6109
d
Te = 29.3 km (7.3 - 40 km)
Java Trench, age = 60-70 Ma
e
Te = 29.3 km, misfit = 1.978
f
Te = 14.8 km (7.2 - 40 km)
Java Trench, age = 80-90 Ma
g
Te = 14.8 km, misfit = 1.725
h
Te = 16.1 km (7.7 - 40 km)
Java Trench, age = 90-100 Ma
i
Te = 16.1 km, misfit = 1.786
j

Figure 21

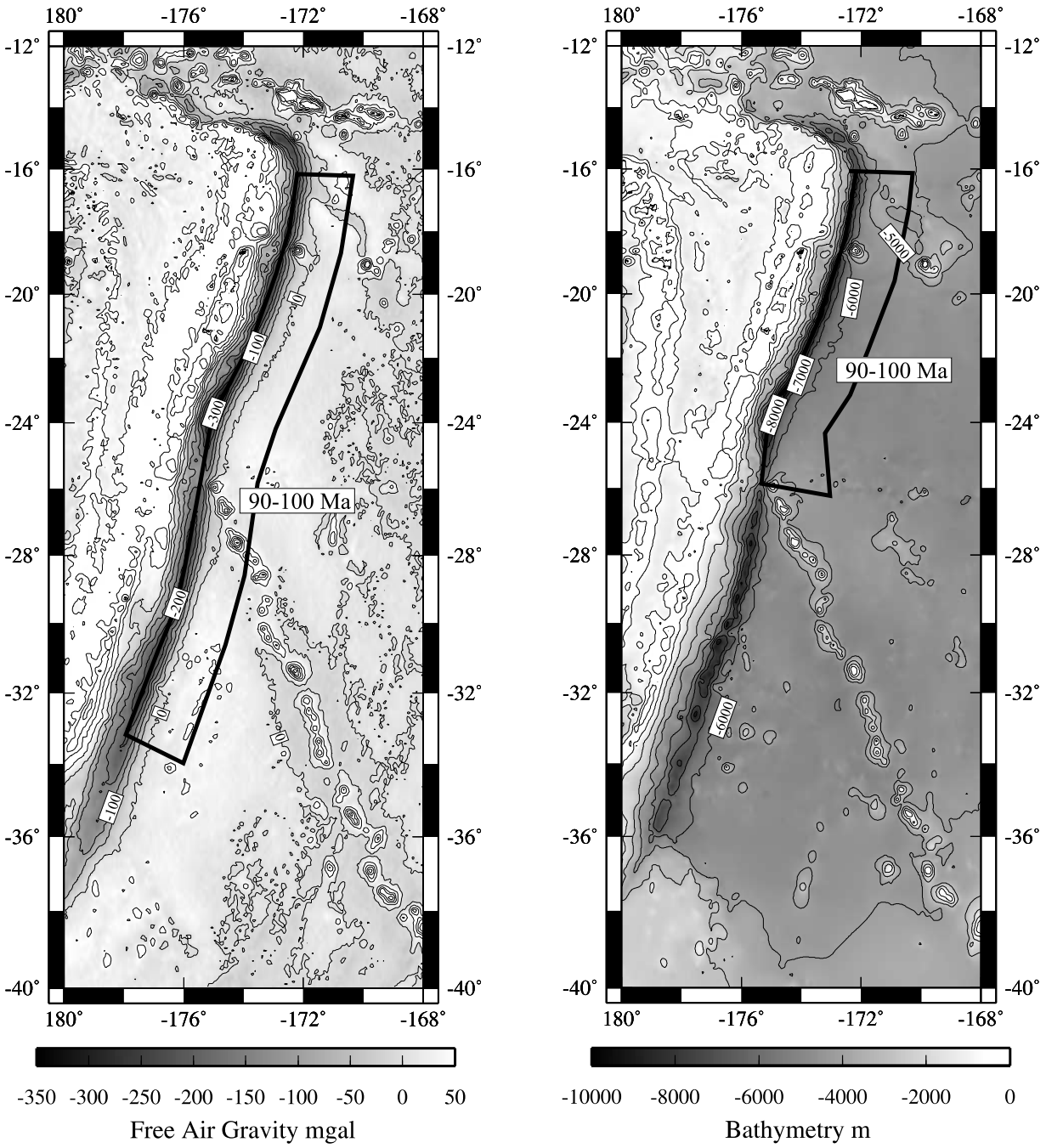

Figure 22. Maps of Tonga Trench. Left-hand panel, free-air gravity map with age-labeled boxes; right-hand panel, bathymetric map with age-labeled boxes.

five sets of free-air gravity results range from ~14 km in the youngest box (40–50 Ma) to ~16 km in the oldest box (90–100 Ma) with a poorly constrained value of T_e for the 60- to 70-Ma region from both gravity and bathymetry (Figure 21). The bathymetric profile for the 40- to 50-Ma section yields a satisfactorily similar result to the free-air gravity result (~13 km), although the profile fit is poor.

3.7. Tonga Trench

[30] Our final set of analyses come from the Tonga Trench which is generated by the subduction of the Pacific

Figure 21. Results of inverse modeling of free-air gravity profiles from Java Trench for five lithospheric plate age ranges shown in Figure 20 (40–50, 50–60, 60–70, 80–90, and 90–100 Ma). (a, c, e, g, and i) Fitted free-air gravity profiles; (b, d, f, h, and j) misfit functions. See caption of Figure 3 for further details.

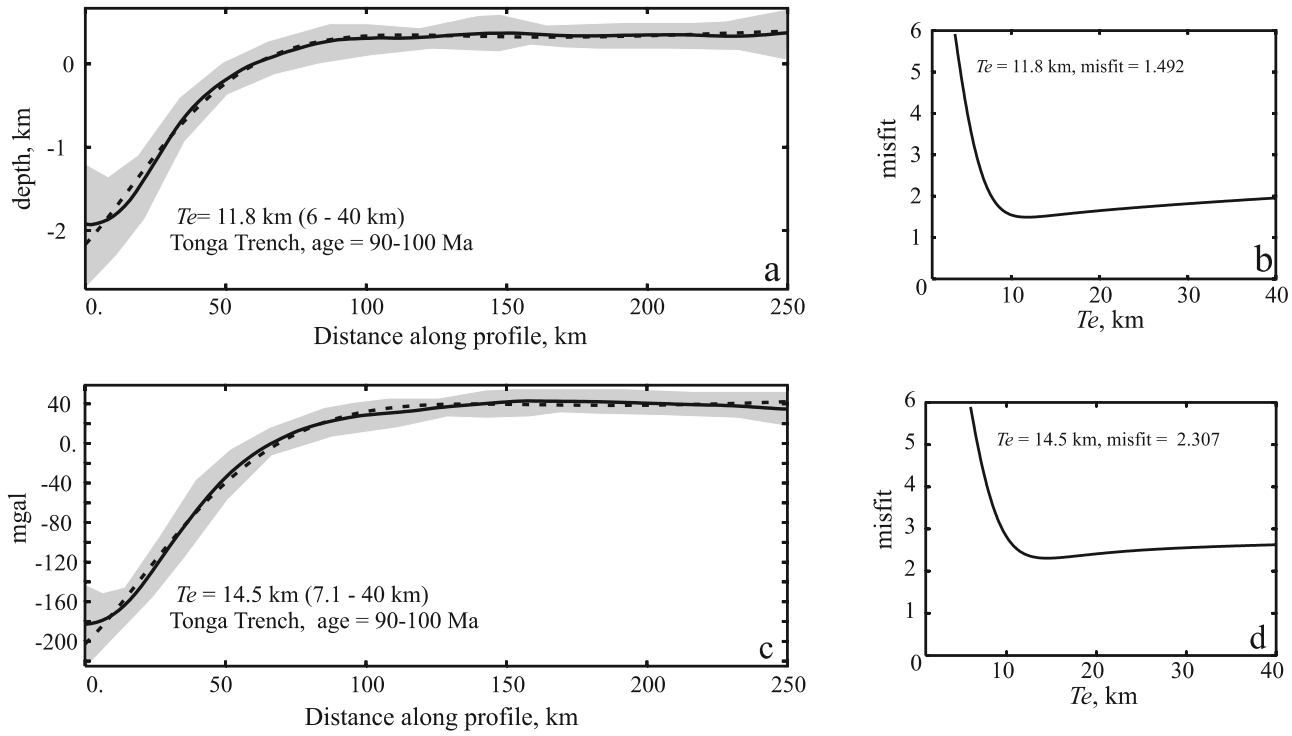

Figure 23. Results of inverse modeling of bathymetric and free-air gravity profiles from Tonga Trench for single lithospheric plate age range shown in Figure 22 (90–100 Ma). (a, c) Fitted free-air gravity profiles; (b, d) misfit functions. See Figure 3 for further details.

Plate beneath the Indo-Australian plate. There is a single box for bathymetry and free-air gravity, ranging from 90 to 100 Ma (Figure 22). Only the northern part of the trench has been adequately sampled by ship tracks. Both T_e values are reasonably similar (12 and 15 km) but neither are well constrained by a deep global minimum (Figure 23). We conclude that these values are the same within error.

4. Discussion

[31] The results obtained for all trenches using bathymetric and free-air gravity profiles are plotted together in Figures 24 and 25 so we can reassess the relationship between T_e and the age of lithosphere adjacent to the trench. T_e values are significantly lower than those obtained by previous workers, which ranged from 15 to 50 km and broadly corresponded to the depths to the 300°–600°C isotherms. Furthermore, our results do not support a convincing relationship between age of lithosphere at time of loading and T_e, regardless of profile length. Instead, T_e values evidently transgress deeper isotherms.

[32] For profile lengths (250–300 km), T_e values obtained using free-air gravity anomalies range from 10 to 20 km; any values which lie outside this range are a consequence of flat misfit functions (Figure 24a). This small range is also reflected in the consistent flexural wavelengths of ~100 km observed at most trenches. Only a very slight increase in T_e values is observed for increasing plate age as follows: The T_e values for the Japan-Marianas Trench have an average of 15 km while those for the younger part of the South American Trench have an average of 9 km. However, it is difficult to infer a significant change in strength between the older and younger trenches from a 5 to 6 km contrast in optimal T_e. Furthermore, the T_e trend cuts across the 300° isotherm (Figure 24). The weak relationship observed for the shorter profiles becomes increasingly scattered when longer profiles (500 and 700 km) are used (Figures 24b and 24c). The pattern of results from bathymetric profiles is generally more inconsistent, probably reflecting the more poorly constrained misfit functions (Figure 25). As with the free-air gravity results, scatter increases for 500-km profile lengths. The results obtained from both the free-air gravity and bathymetry indicate that longer profiles tend to increase the average value of T_e, mainly because misfit functions have flatter minima; longer profiles will reduce the influence of the flexed zone adjacent to the trench and increase the likelihood of including long-wavelength features generated in other ways (for example, dynamic topography). The previous studies of oceanic trenches of *Levitt and Sandwell*

Figure 24. Results obtained by inverse modeling of free-air gravity profiles. Upper panel, profile lengths of 250–300 km; middle panel, profile lengths of 500 km; lower panel, profile lengths of 700 km. Solid and open symbols, values of T_e determined by inverting profiles. Horizontal and vertical error bars are calculated from uncertainties of plate age model and from standard deviations, respectively. Arrows on vertical error bars indicate no lower limit of error bar (lower limit given as 1.25 × minimal misfit). Solid labeled lines, isothermal boundaries from the work of *McKenzie et al.* [2005].

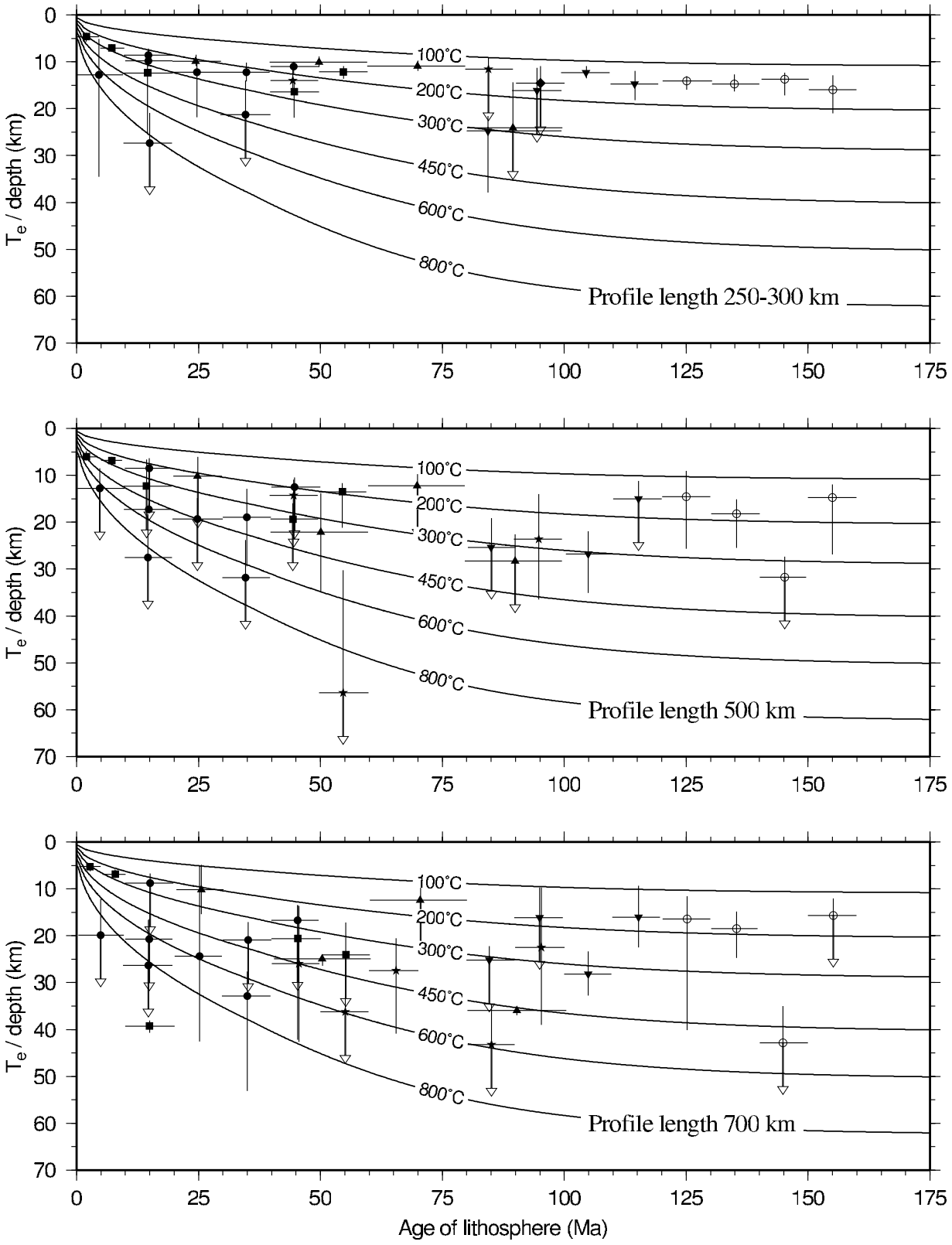
T_e / depth (km)
100°C
200°C
300°C
450°C
600°C
800°C
Profile length 250-300 km
Profile length 500 km
Profile length 700 km
Age of lithosphere (Ma)
Peru-Chile-Central America
Aleutian
Tonga
Java
Kuril-Japan-Marianas
South Sandwich
Caribbean
Upper bound unconstrained

Figure 24

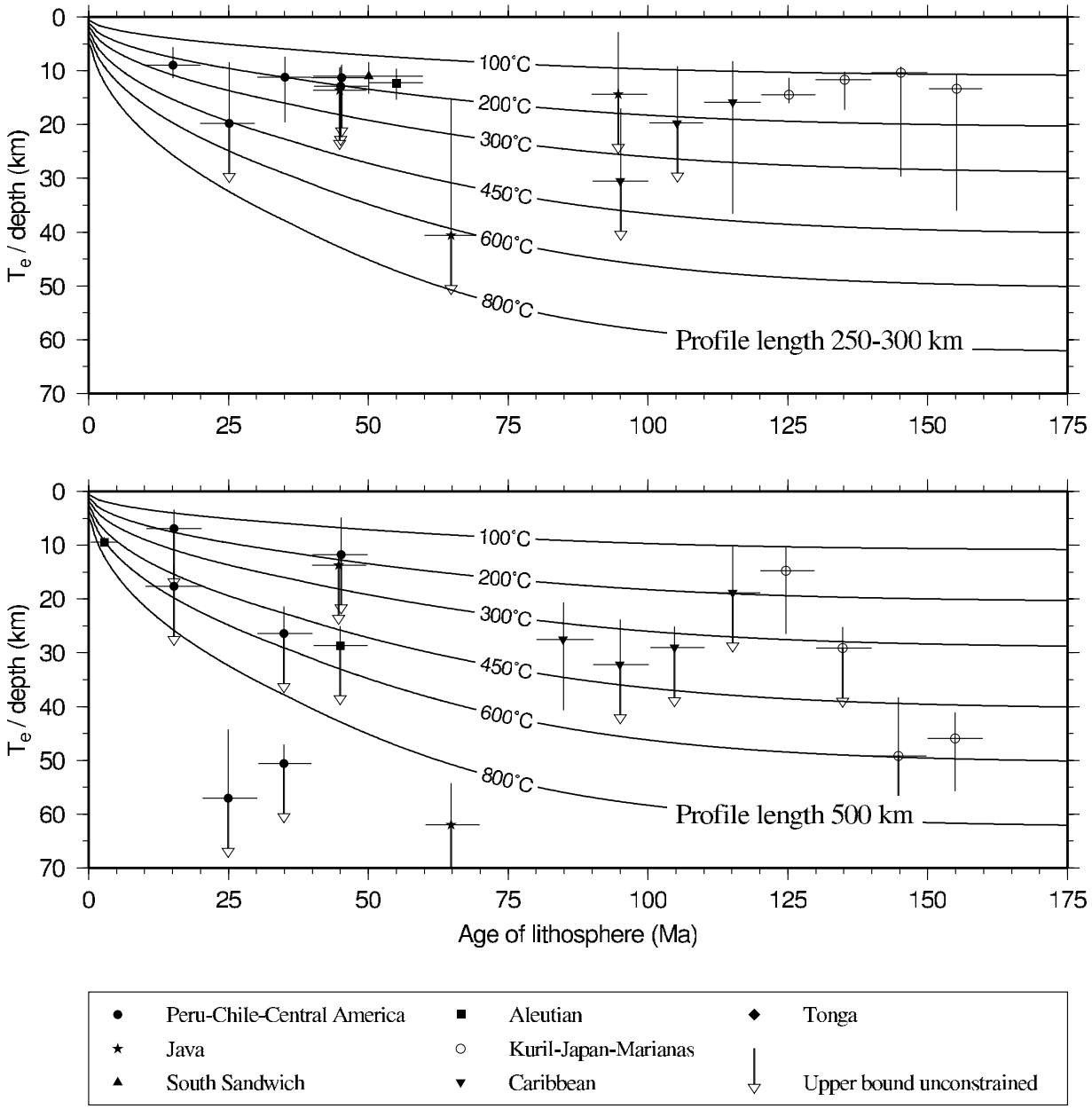

Figure 25. Results obtained by inverse modeling of bathymetric profiles. Upper panel, profile lengths of 250–300 km; lower panel, profile lengths of 500 km. See Figure 24 for further details.

[1995] and *Judge and McNutt* [1991] both used long profile lengths (500–800 km) and individual profiles. The use of shorter averaged profiles here may therefore be the main cause of the smaller T_e values obtained in this study. This inference can be tested by modeling a few individual profiles, taken in the same trenches and with the same coordinates as those in the work of *Levitt and Sandwell* [1995] (Figure 26).

[33] Two individual profiles have been selected for this test. The first one is a profile along the Aleutian Trench with an age of 55 Ma, for which *Levitt and Sandwell* [1995] cited a T_e of ~24 km (Figure 27). Modeling of the deflection over a length of 250 km yields a low T_e value between 9 and 11 km using bathymetry and gravity, respectively. Increasing the profile length to 700 km increases the T_e estimate from each of the data sets to 20 and 26 km, both similar to Levitt and Sandwell's values. However, neither estimate is well constrained. A second profile is taken from the Marianas Trench in order to illustrate the effect of profile length on a 152-Ma section of oceanic crust (Figure 28).

Figure 26. Mechanical thickness values, T_m, plotted as a function of lithospheric plate age. T_m was calculated from gravity-derived estimates of T_e using the ratio of T_m to T_e given as a function of plate curvature [see, e.g., *Watts*, 2001]. Error bars omitted.

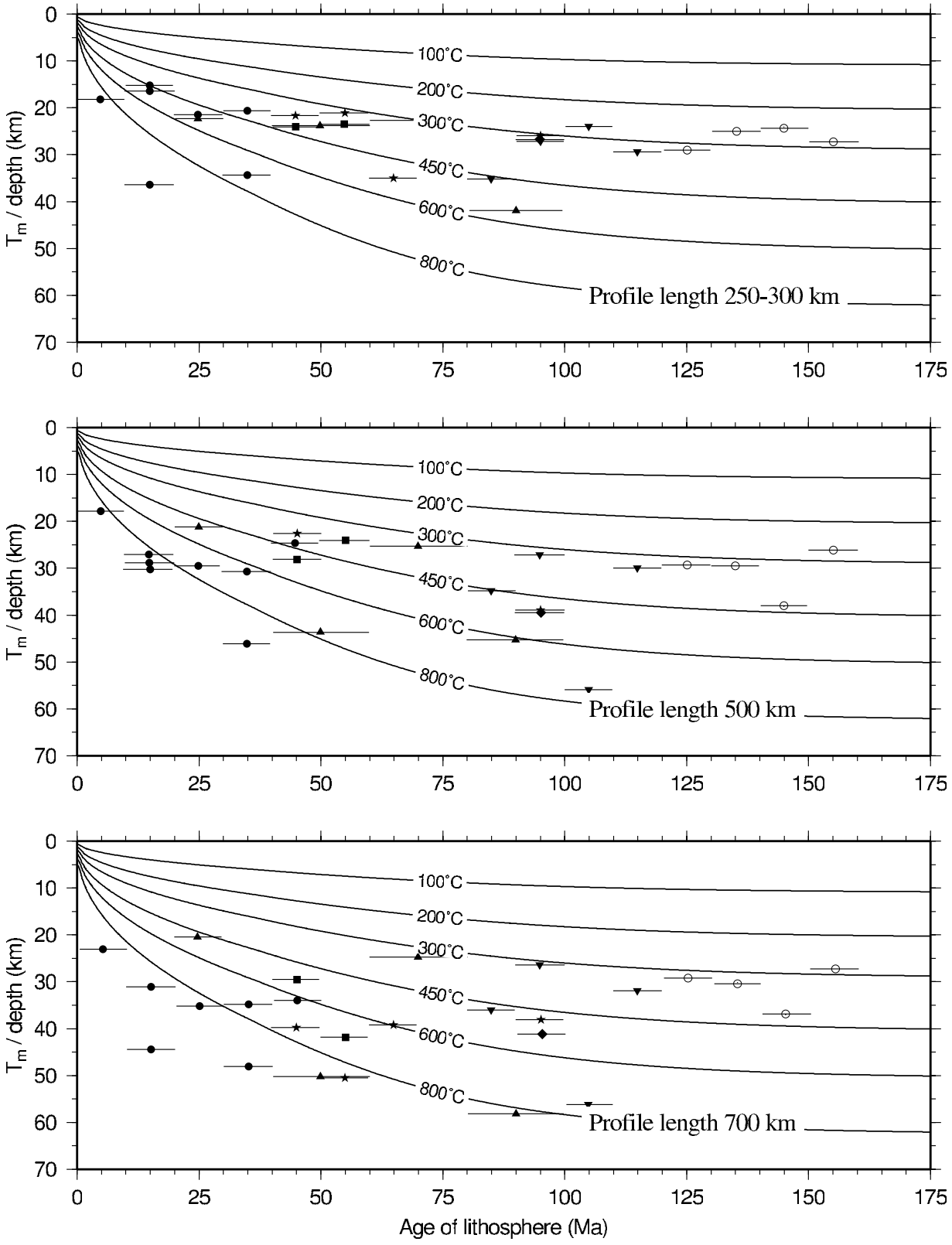
T_m / depth (km)
100°C
200°C
300°C
450°C
600°C
800°C
Profile length 250-300 km
Profile length 500 km
Profile length 700 km
Age of lithosphere (Ma)
Peru-Chile-Central America
Aleutian
Tonga
Java
Kuril-Japan-Marianas
South Sandwich
Caribbean

Figure 26

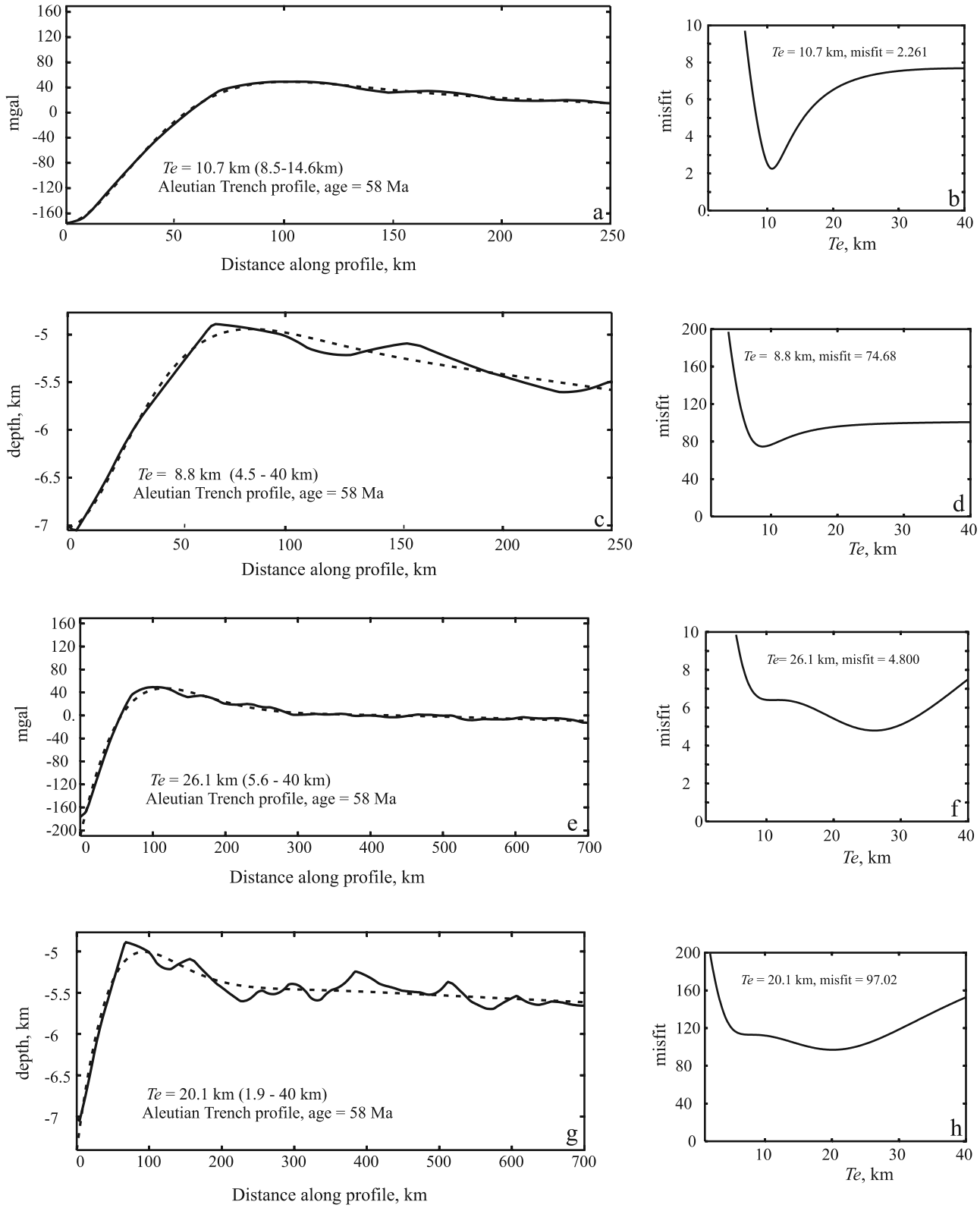

Figure 27. Inverse modeling of individual bathymetric and free-air gravity profiles from Aleutian Trench for which *Levitt and Sandwell* [1995] obtained T_e = 24.3 km (800 km profiles). (a, b) Fitted free-air gravity profile (250 km long) and misfit function for 58-Ma lithosphere; (c, d) fitted bathymetric profile (250 km long) and misfit function for 58-Ma lithosphere; (e, f) Fitted free-air gravity profile (700 km long) and misfit function for 58-Ma lithosphere; (g-h) fitted bathymetric profile (700 km long) and misfit function for 58-Ma lithosphere. Note that estimate and uncertainty of T_e is strongly dependent upon profile length.

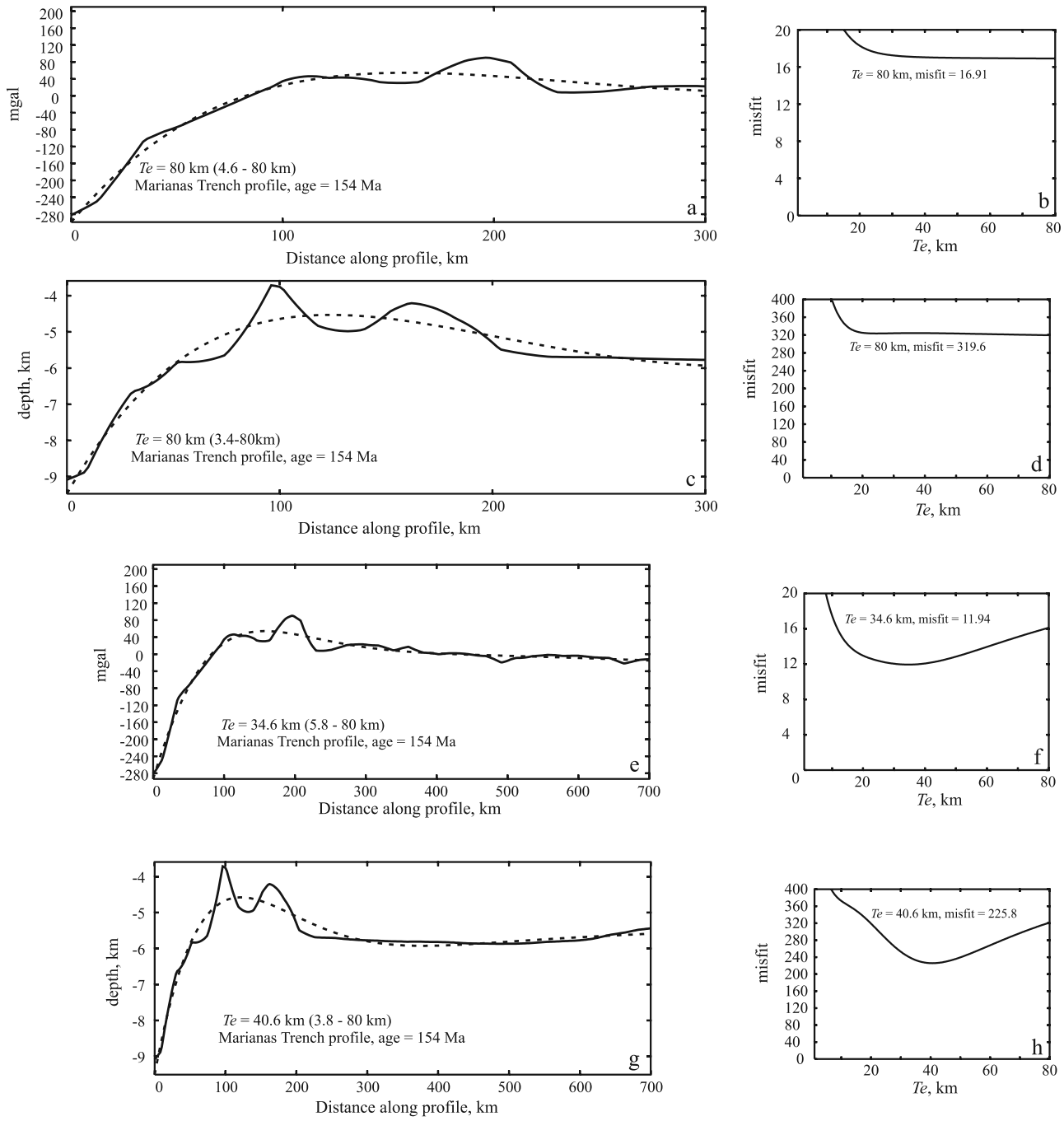

Figure 28. Inverse modeling of individual bathymetric and free-air gravity profiles from Aleutian Trench for which *Levitt and Sandwell* [1995] obtained T_e = 38.6 km (800 km profiles). (a, b) Fitted free-air gravity profile (250 km long) and misfit function for 154-Ma lithosphere; (c, d) fitted bathymetric profile (250 km long) and misfit function for 154-Ma lithosphere; (e, f) Fitted free-air gravity profile (700 km long) and misfit function for 154-Ma lithosphere; (g, h) fitted bathymetric profile (700 km long) and misfit function for 154-Ma lithosphere. Note that estimate and uncertainty of T_e is strongly dependent upon profile length.

The estimate of *Levitt and Sandwell* [1995] for this profile is ~39 km. This profile illustrates the problems encountered when modeling individual deflections, which are, in this case, caused by a set of oceanic islands located close to the flexural bulge of the deflection. In this case, a prominent seamount forces T_e to be unconstrained because it disrupts the slope of the deflection on short profiles. A longer profile produces a more satisfactory fit since only a small proportion of the profile is affected by the seamount, yielding similar results to those found by *Levitt and Sandwell* [1995]. This problem has been sidestepped by averaging profiles for

the modeling of the 150- to 160-Ma-age section (Figure 19 and 18).

[34] Maximum curvatures calculated for every trench profile yield values $\sim 10^{-7}$ m^{-1}, which are believed to be large enough to induce inelastic failure. Many authors have suggested that elastic thicknesses calculated for plates with such large curvatures underestimate the true mechanical thickness of the plate since inelastic failure effectively reduces the thickness of the layer which can transmit elastic stresses. Our calculated T_e values are easily converted into mechanical thickness values, T_m, using the ratio of T_m to T_e against curvature [*McNutt and Menard*, 1982]. This conversion into mechanical thickness has adherents and detractors, and we do not wish to rehearse contentious and unresolved arguments here. We simply point out that the results of this conversion do not improve the relationship between T_e and plate age. The majority of T_m values certainly fall between the 300° and 600°C isotherms for the shortest profile lengths but a strength-age relationship is not evident (Figure 26a). The relationship between T_m and plate age becomes increasingly scattered for longer profile lengths, highlighting the uncertainty which results from choosing different profile lengths. Shorter profiles yield more satisfactory fits to the deflections and better constrained misfit functions because they sample the zone where plate curvature is greatest. Longer profiles sample more of the long wavelength outer rise and so place less emphasis on the zone of greatest curvature. This difference could be accounted for by decreasing elastic thickness toward the trench. We are reluctant to complicate our model in this way since all profiles can be fitted accurately with uniform values of T_e. Selection of profile length remains a fundamental uncertainty in T_e modeling.

[35] We are surprised that our results do not support a simple relationship between plate strength and age. There are two possible explanations. First, estimates of T_e are too uncertain to show a relationship which can be confidently inferred on rheological grounds alone. At best, we would concur with *McQueen and Lambeck* [1989], who, on the basis of a much smaller data set, suggested that, while T_e values had large uncertainties, they did appear to track, albeit roughly, the 200°C isotherm, which would correspond to a homologous temperature of 0.4 for wet peridotite. Second, no relationship between elastic thickness and plate age exists. Instead, plate bending may be strongly modulated by shear failure, by changes in plate thickness, and by phase changes. Our null relationship has profound consequences for the long-accepted relationship between plate strength and thermal history in both oceans and continents.

[36] Finally, it is instructive to compare our results with newly published T_e estimates obtained from seamounts. *Watts et al.* [2006] obtained 9758 estimates of T_e by analyzing submarine features. They also conclude that there is no simple relationship between T_e and age. Instead, T_e varies between 5 and 30 km regardless of age with an average value is 18 ± 11 km. *Crosby* [2006] analyzed a smaller number of well-studied seamounts where the age at time of loading is better constrained. His estimates also show that T_e varies unsystematically between about 5 and 30 km. Thus trenches and seamounts yield a suite of self-consistent results, which suggests that the lack of a relationship between plate strength and age is general throughout the oceanic realm. The absence of such a relationship questions the value of elastic thickness estimates. Are we measuring the wrong parameter?

[37] **Acknowledgments.** MB was funded by the University of Cambridge European Trust and by St. John's College. We are grateful to D. McKenzie who generously allowed us to use and to modify his flexural software as well as making many useful suggestions. D. Sandwell kindly provided ship track data, and A. Crosby generated Figures 24, 25, and 26. We have also benefited from numerous discussions with A. Crosby, J. Jackson, C. Lightfoot, F. Nimmo, A. Watts, R. White. P. Elosegui, and D. Forsyth, and an anonymous referee wrote thoughtful reviews and suggested many improvements although the usual disclaimer applies. ES contribution 8765.

References

Ashby, M. F., and R. A. Verrall (1977), Micromechanisms of flow and fracture, and their relevance to the rheology of the upper mantle, *R. Soc. London Philos. Trans. Ser. A*, *288*, 59–95.

Bodine, J. H., M. S. Steckler, and A. B. Watts (1981), Observations of flexure and the rheology of the oceanic lithosphere, *J. Geophys. Res.*, *86*, 3695–3707.

Burov, E. B., and M. Diament (1995), The effective elastic thickness (T_e) of continental lithosphere: What does it really mean?, *J. Geophys. Res.*, *100*, 3905–3927.

Caldwell, J. G., and D. L. Turcotte (1979), Dependence of the thickness of the elastic oceanic lithosphere on age, *J. Geophys. Res.*, *84*, 7572–7576.

Caldwell, J. G., W. F. Haxby, D. E. Karig, and D. L. Turcotte (1976), On the applicability of a universal elastic trench profile, *Earth Planet. Sci. Lett.*, *31*, 239–246.

Calmant, S. (1987), The elastic thickness of the lithosphere in the Pacific Ocean, *Earth Planet. Sci. Lett.*, *85*, 277–288.

Cloetingh, S., and E. B. Burov (1996), Thermomechanical structure of European continental lithosphere: Constraints from rheological profiles and EET estimates, *Geophys. J. Int.*, *124*, 695–723.

Courtney, R. C., and C. Beaumont (1983), Thermally activated creep and flexure of the oceanic lithosphere, *Nature*, *305*, 201–204.

Crosby, A. (2006), Aspects of the relationship between topography and gravity on the Earth and its Moon, Ph.D. dissertation, Univ. of Cambridge.

De Bremaecker, J. C. (1977), Is the oceanic lithosphere elastic or viscous?, *J. Geophys. Res.*, *82*, 2001–2004.

Forsyth, D. W. (1980), Comparison of mechanical models of the oceanic lithosphere, *J. Geophys. Res.*, *85*, 6364–6368.

Goetze, C., and B. Evans (1979), Stress and temperature in the bending lithosphere as constrained by experimental rock mechanics, *Geophys. J. R. Astron. Soc.*, *59*, 463–478.

Jordan, T. A., and A. B. Watts (2005), Gravity anomalies, flexure and the elastic thickness structure of the Indian-Eurasia collisional system, *Earth Planet. Sci. Lett.*, *236*, 732–750.

Judge, A. V., and M. K. McNutt (1991), The relationship between plate curvature and elastic plate thickness: A study of the Peru-Chile trench, *J. Geophys. Res.*, *96*, 16,625–16,640.

Kaplan, R. W. Wiener, and I. O. Norton (1985), Tectonic Map of the World. Exxon Production Research Company.

Levitt, D. A., and D. T. Sandwell (1995), Lithospheric bending at subduction zones based on depth soundings and satellite gravity, *J. Geophys. Res.*, *100*, 379–400.

McAdoo, D. C., and C. F. Martin (1984), Seasat observations of lithospheric flexure seaward of trenches, *J. Geophys. Res.*, *89*, 3201–3210.

McAdoo, D. C., C. F. Martin, and S. Poulose (1985), Seasat observations of flexure: Evidence for a strong lithosphere, *Tectonophysics*, *116*, 209–222.

McKenzie, D., and D. Fairhead (1997), Estimates of the effective elastic thickness of the continental lithosphere from Buoguer and free-air gravity anomalies, *J. Geophys. Res.*, *102*, 27,523–27,552.

McKenzie, D., J. Jackson, and K. Priestley (2005), Thermal structure of oceanic and continental lithosphere, *Earth Planet. Sci. Lett.*, *233*, 337–349.

McNutt, M. K. (1984), Lithospheric flexure and thermal anomalies, *J. Geophys. Res.*, *89*, 11,180–11,194.

McNutt, M. K., and H. W. Menard (1982), Constraints on yield strength in the oceanic lithosphere derived from observations of flexure, *Geophys. J. R. Astron. Soc.*, *71*, 363–394.

McQueen, H. W. S., and K. Lambeck (1989), The accuracy of some lithospheric bending parameters, *Geophys. J. Int.*, *96*, 401–413.

Müller, R. D., W. R. Roest, J.-Y. Royer, L. M. Gahagan, and J. G. Sclater (1997), Digital isochrons of the world's ocean floor, *J. Geophys. Res.*, *102*, 3211–3214.

Parsons, B., and P. Molnar (1976), The origin of outer topographic rises associated with trenches, *Geophys. J. R. Astron. Soc.*, *45*, 707–712.

Parsons, B., and J. G. Sclater (1977), An analysis of the variation of oceanic floor bathymetry and heat flow with age, *J. Geophys. Res.*, *82*, 803–827.

Press, W. H., B. P. Flannery, S. A. Teukolsky, and W. T. Vetterling (1986), Numerical Recipes—The art of Scientific Computing, Cambridge Univ. Press, New York, 817 pp.

Roest, W. R., R. D. Müller, J.-Y. Royer, and L. M. Gahagan (1992), A high resolution digital age map of the world's oceans, *EOS Trans. AGU*, *73*, 586.

Sandwell, D. T., and W. H. F. Smith (1992), Global marine gravity from ERS-1, Geosat and Seasat reveals new tectonic fabric, *EOS Trans. AGU*, *73*, 133.

Stein, C. A., and S. Stein (1992), A model for the global variation in oceanic depth and heat flow with lithospheric age, *Nature*, *359*, 123–129.

Turcotte, D., and G. Schubert (1982), Geodynamics: Applications of Continuum Physics to Geological Problems, 450 pp., John Wiley, Hoboken, N. J.

Watts, A. B. (1978), An analysis of isostasy in the world's oceans: 1. Hawaiian-Emperor seamount Chain, *J. Geophys. Res.*, *83*, 5989–6004.

Watts, A. B. (2001), Isostasy and Flexure of the Lithosphere, 458pp., Cambridge Univ. Press, New York.

Watts, A. B., and S. Zhong (2000), Observations of flexure and rheology of oceanic lithosphere, *Geophys. J. Int.*, *142*, 855–875.

Watts, A. B., J. H. Bodine, and M. S. Steckler (1980), Observations of flexure and the state of stress in the oceanic lithosphere, *J. Geophys. Res.*, *85*, 6369–6376.

Watts, A. B., D. T. Sandwell, W. H. F. Smith, and P. Wessel (2006), Global gravity, bathymetry and the distribution of submarine volcanism through space and time, *J. Geophys. Res.*, *111*, B08408, doi:10.1029/2005JB004083.

Weertman, J. (1978), Creep laws for the mantle of the Earth, *Philos. Trans. R. Soc. London Ser. A*, *288*, 9–26.

Westbrook, G. K. (1982), The Barbados Ridge complex: Tectonics of a mature forearc system. In Trench-Forearc Geology, edited by J. K. Leggett, *Geol. Soc. London Spec. Publ., 10*, 275–290.

M. Bry and N. White, Bullard Laboratories, Department of Earth Sciences, University of Cambridge, Madingley Rise, Madingley Road, Cambridge, CB3 0EZ, UK. (nwhite@esc.cam.ac.uk)